EXHIBIT V

PART 18

34

Wall Slip in Viscous Fluids and Influence of Materials of Construction

A. V. RAMAMURTHY, *Union Carbide Corporation, P. O. Box 670, Bound Brook, New Jersey 08805*

Synopsis

The question of slip and the influence of materials of construction on the observed extrudate irregularities are examined for high viscosity molten polyethylenes. Capillary rheometer studies were conducted for several linear (LLDPE and HDPE) and branched (HP-LDPE) polyethylenes, Viton A, and Barex-210. Extensive blown film fabrication studies were conducted for narrow MWD UNIPOL process LLDPE resins. The results indicate that the assumption of "no-slip at the rigid boundary" is generally not valid for polyethylenes above a critical shear stress of approximately 0.1–0.14 MPa, when either surface or gross irregularities are present in the extrudate. Loss of extrudate gloss at the critical shear stress defines the onset of melt fracture. Within the range of variables examined, the critical stress is relatively insensitive to molecular characteristics (molecular weight, MWD, and chain branching), melt temperature, and the detailed design of the capillary. Contrary to capillary rheometer observations, blown film fabrication results for LLDPE indicate that materials of construction for the die land region have a significant influence on melt fracture, and suggest breakdown of adhesion at the polymer/metal interface as a primary cause of slip and melt fracture. The results demonstrate that methods to improve adhesion, by proper choice of materials of construction for the die land region and/or use of adhesion promoters in the resin, virtually eliminate the rate-limiting effects of melt fracture in commercial blown film fabrication. The results highlight a deficiency of standard capillary rheometer methods to delineate the influence of materials of construction and/or adhesion promoters on observed melt fracture characteristics with molten polyethylenes.

INTRODUCTION

Extrudate irregularities, commonly referred to as *melt fracture*, occur at low deformation rates with some polymers, such as the narrow molecular weight distribution (MWD) linear low-density polyethylenes (LLDPE). With large-scale commercial use and

© 1986 by The Society of Rheology, Inc. Published by John Wiley & Sons, Inc.
Journal of Rheology, 30(2), 337–357 (1986) CCC 0148-6055/86/020337-21$04.00

as linear polymers are concerned. It is almost certain that slip is negligible for branched polymers."

In contrast to studies on gross melt fracture, surface melt fracture has received less attention, although it has been observed, to varying degrees, with a wide range of polymers including HDPE,[8] HP-LDPE,[9] and PVC.[10] The literature suggests that surface melt fracture is a die exit phenomenon and occurs as a consequence of high local stresses as the viscoelastic melt parts company with the die. That is, surface melt fracture is distinctly different from gross melt fracture which is a die-entry and/or a die-land effect. The possibility of slip in the die land region under surface melt fracture conditions has not been considered.

This paper focuses attention on some results which may be useful in resolving the question of slip in the die land region for polyethylenes in general, and for linear polymers such as HDPE and LLDPE in particular. The influence of materials of construction on the observed extrudate irregularities is examined in both capillary and blown film fabrication situations.

EXPERIMENTAL

A capillary rheometer, built by the R&D team at Union Carbide, was used for studies to determine the flow curves and extrudate characteristics of molten polymers. Capillary dies (orifice dimensions: 0.5–2.5 mm diameter, 2–20 L/D, and 60–180° included angle) constructed from SAE 4140 steel were employed. Abrupt entry dies (1 mm diameter and 20 L/D) of various metals were used to study the influence of materials of construction on extrudate characteristics for LLDPE resins. A stepwise regression was used to fit the steady-state data to a power–law model. Particular attention was paid to determine the conditions for the onset of surface (loss of gloss) and gross melt fracture.

A wide range of linear (HDPE and LLDPE) and branched (HP-LDPE) polyethylenes (see Table I for nominal characteristics) were studied. The characteristics of two other commercial polymers, Barex-210 (a copolymer of acrylonitrile and methylmethacrylate, supplied by Vistron Corporation) and Viton A (a fluoroelastomer, supplied by E. I. duPont de Nemours & Co., Inc.), were also examined.

Blown film fabrication studies were conducted with a 50 mm,

TABLE I
Nominal Characteristics of Polyethylenes Studied

Type	MI or range studied (dg/min)	MFR	Density (kg/m³)	MW/Mn
LLDPE[a]	0.2–20	26	918	3.9
LLDPE[b]	0.2–2	26	918	3.9
HDPE[a,b]	1.0	26	950	3.9
HDPE[a]	1.3	39	950	7.9
HP-LDPE[a,b]	2	65	920	14.0
HP-LDPE[a,b]	0.1	128	917	11.8

[a] Capillary studies.
[b] Blown film studies.

24/1 L/D extruder fitted with a 75 mm spiral die of standard hard chrome-plated steel construction, and a dual lip air ring for bubble cooling. The influence of construction materials for the die land region on melt fracture in the film was studied. For this, a modified mandrel design (Fig. 2) was constructed to allow use of metal inserts. Using standard fabrication procedures, 38 μm films were fabricated. The onset of melt fracture was determined by visual examination of the film. Surface roughness measurements with a Bendix Proficorder (Bendix Corporation, Southfield,

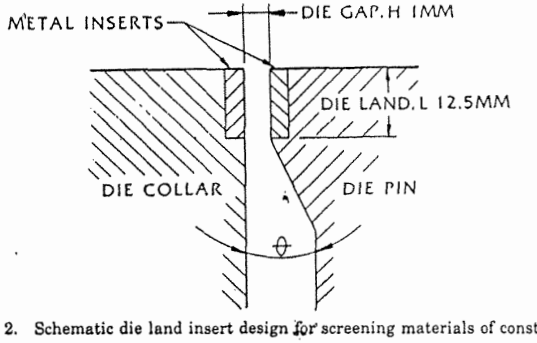

Fig. 2. Schematic die land insert design for screening materials of construction.

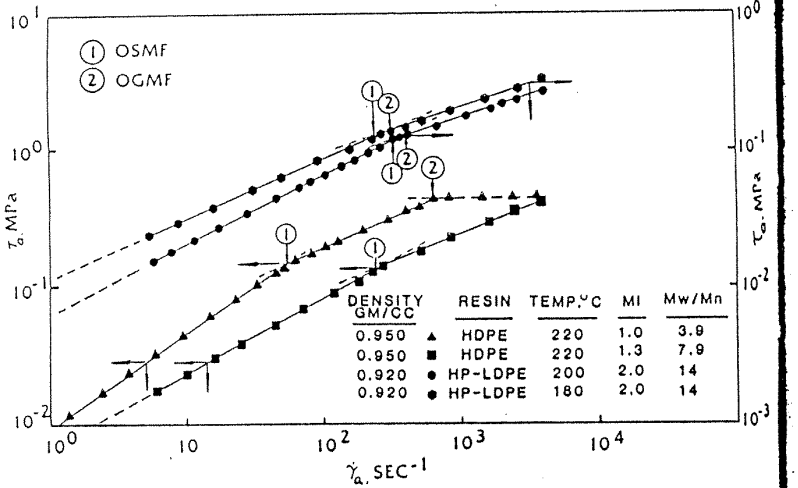

Fig. 3. Apparent flow curves for HP-LDPE and HDPE resins. Capillary: 1 mm diameter, and 20 L/D with abrupt entry.

MWD and for a HP-LDPE with broad MWD at two temperatures. Table II includes the power-law constants for these resins. The results demonstrate that, not only does surface melt fracture occurs with HP-LDPE, but, the change in slope of the flow curve at the onset of surface melt fracture occurs at a reasonably constant critical shear stress (τ_{c1}: 0.12–0.14 MPa), independent of the structure and melt temperature for polyethylenes in general. Note, however, that the shear stress for the onset of gross melt fracture (0.13 MPa) with HP-LDPE is extremely close to that for surface melt fracture.[11] In comparison, the corresponding shear stresses (0.14 and 0.43 MPa) for linear polyethylenes are widely separated.[11] Thus, if one adopts loss of extrudate gloss as the condition for denoting the onset of extrudate irregularities, the critical shear stress becomes independent of the molecular characteristics and melt temperature for polyethylenes. This seems reasonable, since any departure from smooth and glossy condition should be regarded as an undesirable feature.

An examination of the published flow curves for polyethylenes reveals, in many cases, a change in slope around a shear stress of approximately 0.1–0.14 MPa, above and below which a power-law model could be used to accurately represent the steady-state data. For example, the apparent flow curve presented by Lupton and Register[11] for a narrow MWD 1 MI HDPE at 190°C shows a change in slope (from about 0.59 to 0.4) at a shear stress of 0.14 MPa, similar to that in Figure 1 for LLDPE. The composite flow curve presented by Metzner et al.[12] for an HP-LDPE at 160°C shows a change in slope (from about 0.49 to 0.32) around a shear stress of 0.12 MPa. Also, slope changes at a wall shear stress of approximately 0.1 MPa can be seen in the tabulated corrected data of Bagley[13] for both HDPE and HP-LDPE. It is difficult, however, to determine from the published data if these investigators observed any surface irregularities at stresses corresponding to the change in slope.

In contrast to the polyethylenes, the capillary rheometer results for Viton A and Barex-210 (see Fig. 4) indicate that these polymers exhibit neither any change in slope nor any susceptibility to melt fracture at stresses substantially higher than those for the polyethylenes. Thus, it is important to determine the basic cause of the change in slope of the steady flow curve at the onset of surface melt fracture with polyethylenes. The generally accepted mechanism in the literature for surface melt fracture, based on die exit effects, fails to explain either the change in slope or the increased shear thinning behavior with linear polyethylenes. Since the apparent shear stress is calculated using the total length of the die, these results may be explained if one considers the possibility of slip in the die land region above the critical stress τ_{c1}, even under steady conditions for surface melt fracture.

Figure 5 presents standard measurements, with a series of capillary dies (0.5–2.5 mm diameter, 20 L/D abrupt entry) of 4140 steel, for determining the validity of the no-slip assumption under steady flow conditions for the 1 MI LLDPE at 220°C. It indicates that the no-slip assumption is valid at apparent shear stresses below 0.1 MPa, corresponding to smooth and glossy extrudates. However, at a shear stress of 0.1 MPa, which is slightly below that for the loss of gloss, the measured shear rate shows some dependence on the capillary radius (R) indicating slip at the wall (slip velocity, v_s: 0.61 mm/sec). At the critical stress (0.14

Case 1:05-cv-00737-JJF Document 160-5 Filed 09/03/2008 Page 5 of 42

EXHIBIT PAGE 000980

TABLE III
Measured Power-Law Constants with Some Die Materials 1 MI LLDPE; 220°C

	Capillary: 1 mm × 20 L/D					
Metal	n_1	K_1	n_2	K_2	τ_{c1}	τ_{c2}
Aluminum (6061-T6)	0.61	1.47	0.41	3.30	13.7	39.1
Beryllium copper	0.55	1.54	0.42	2.41	10.4	37.7
Carbon steel (SAE 4140)	0.64	0.93	0.46	1.95	14.4	43.5
Carbon steel (SAE 4340)	0.64	0.93	0.46	1.95	14.4	43.5
CDA 360[a]	0.62	1.05	0.39	2.96	17.2	41.3
CDA 464[a]	0.64	0.98	0.44	2.31	15.3	40.7
Bronze (Ampco 45)	0.61	1.20	0.44	2.43	14.6	43.4
Copper	0.61	0.99	0.44	2.09	13.2	41.5
Stainless steel (304)	0.65	1.01	0.46	2.32	15.1	44.1

Subscript 1 refers to smooth and glossy conditions.
Subscript 2 refers to conditions above τ_{c1}.
K is expressed in Pa·sec^n × 10^{-4}.
Critical stress values expressed in Pa × 10^{-4}.
[a]Copper Development Association designations.

Nominal compositions, %:	Cu	Zn	Pb	Sn
CDA-360:	61.5	35.5	3.0	—
CDA-464:	60.0	39.2	—	0.8

fracture, is less dependent on the materials of construction, which is consistent with the reported observations of Tordella, and Metzger and Hamilton for HDPE. However, as the results to follow indicate, the influence of the materials of construction for the die land region under blown film fabrication conditions is entirely different from that indicated by the capillary rheometer results.

Blown Film Fabrication Studies

Table IV lists observations to illustrate the rate-limiting effects of melt fracture with a 1 mm die gap of conventional chrome-plated steel configuration. For the 1 MI LLDPE, melt fracture in the film occurs at an uneconomically low rate of extrusion (0.41 kg/hr per cm of die circumference). At commercial rates of 1.5–2 kg/hr per cm, narrow gap extrusion results in unacceptable products, due to severe melt fracture, as indicated by the measured surface roughness. It may be noted that the shear rate for the onset of melt fracture, under film fabrication conditions, is higher

TABLE IV
Effects of Extrusion Rate on Melt Fracture for 1 MI LLDPE—Conventional Chrome-Plated Steel Surfaces

Equipment: 50 mm, 24/1 L/D extruder; 75 mm spiral die with hard chrome-plated 4140 steel surfaces; dual lip air ring

Conditions:					
Die gap, mm		1.0	1.0	1.0	1.0
Land length/gap		12.5	12.5	12.5	12.5
Die rate, kg/hr/cm		0.34	0.48	0.94	1.37
$\dot{\gamma}_a$ (slit), 1/sec		73.7	102	200	290
Melt temp., °C		215	220	220	220
BUR		2:1	2:1	2:1	2:1
Film thickness, μm		38	38	38	38
Observations:					
Melt fracture		None	Onset[a]	High	Severe
Roughness, μm	MD	0.05	0.41	0.46	0.51
	TD	0.05	0.66	1.07	1.51

MD—Machine direction.
TD—Transverse direction.
[a]—Onset determined by visual examination.

(about 100 1/sec) than that (about 60 1/sec) predicted from Eq. (1) for capillary dies.

Blown film fabrication experiments were conducted with a modified design of the mandrel extension region (see Fig. 2) to allow use of metal inserts for the die land region. Note that the rest of the die, including the die entry, was constructed from conventional chrome-plated steel. Several metals (ferrous and nonferrous) and coatings were examined for the 1 MI LLDPE under identical extrusion conditions. The die land surfaces were visually examined, before and after extrusion, for any discernible changes in the surface appearance.

Table V lists qualitative observations with some representative die land surfaces. These illustrate, contrary to the capillary rheometer observations, a significant influence of the materials of construction on melt fracture under continuous, film-blowing conditions. At identical fabrication conditions, films with melt fracture may appear qualitatively similar. However, the details of film surface (roughness, ridge amplitude, and ridge separation) are a function of the nature of the die land surface. For example, films fabricated with titanium nitride coating exhibited the most

TABLE VI
Performance Comparison of CDA-360 with Chrome-Plated Steel

Equipment: 50–115 mm extruders; 75–300 mm spiral dies; appropriate air rings
Resin: 1 MI LLDPE

Surface	Chromé-plated 4140			CDA-360*		
Die gap, mm	1.0	1.0	1.0	0.5	0.125	
L/H	12.5	12.5	12.5	12.5	5.0	
Entry angle, degrees	7.5	7.5	7.5	7.5	7.5	
Die rate, kg/hr/cm	0.48	1.4	0.5–3.0	0.5–3.3	0.5–1.7	
Melt temp., °C	220	220	200–230	200–230	220	
Shear rate, 1/sec	102	303	106–650	423–2840	6770–23400	
Induction time, min	—	—	40	25	10	
Melt fracture	Onset	Severe	None	None	None	

*Observations following induction period.

available results (not presented here), indicate that within the range of variables examined, the equilibrium performance of CDA-360 is independent of the gap, land length to gap ratio (L/H), extrusion rate, and melt temperature for a wide range of resins. The induction time is dependent on the shear rate in the die land region. Higher shear rates generally require shorter induction time. An important point illustrated by Table VI (note the shear rate ranges with 1 and 0.5 mm gaps) is that, for the 1 MI LLDPE, no melt fracture was observed with CDA-360 at shear rates in excess of 20,000 1/sec, which totally contradicts the capillary rheometer observations with CDA-360 (Table III). Since specific time-dependent interfacial effects are involved, it seems clear that standard capillary rheometer methods are unable to provide useful information for delineating the influence of materials of construction on the extrudate irregularities with molten polymers.

BASIC METHODS FOR ELIMINATION OF MELT FRACTURE

The results of the present studies indicate that the die land region is the primary site of initiation, and slip due to breakdown of adhesion at the polymer/metal interface is the primary cause of the observed extrudate irregularities with polyethylenes. Thus, methods to improve adhesion at the interface in the die land region would essentially eliminate the rate-limiting effects of melt fracture in commercial blown film fabrication. The necessary chemical forces for good adhesion can be achieved by either proper choice of the materials of construction,[16] or use of adhesion promoters in the resin, or an optimum combination of both.[14] The influence of the materials of construction for the die land region is clear from the above film fabrication studies and will not be discussed further.

Adhesion Promoters

There are several polymers and low molecular weight additives which, although not recognized as such, improve adhesion of melt fracture prone polyethylenes to even conventional chrome-plated die surfaces. Included here are additives, normally referred to as

sumption is limited to a certain critical shear stress below which the extrudates are smooth and glossy. The assumption is not valid when either surface or gross irregularities are present.

2. Loss of extrudate gloss and the initiation of slip in the die land region occur at a critical shear stress of approximately 0.1–0.14 MPa, and denotes the condition for onset of extrudate irregularities.

3. Within the range of variables examined, the critical shear stress is independent of the molecular structure (molecular weight, MWD, and branching), melt temperature, and the detailed design of the capillary.

4. Breakdown of adhesion at the polymer/metal interface in the die land region at the critical stress appears to be primarily responsible for the initiation of slip and the observed extrudate irregularities.

5. Under continuous blown film fabrication conditions, methods to provide good adhesion at the polymer/metal interface, by proper choice of the materials of construction for the die land region and/or use of adhesion promoters in the resin, essentially eliminate the rate-limiting effects of melt fracture.

6. Standard capillary rheometer methods are unable to delineate the influence of materials of construction and/or adhesion promoters on melt fracture behavior of polyethylenes. The influence of such variables should be determined under actual fabrication conditions.

The author wishes to thank Union Carbide Corporation for permission to publish this work. The author is extremely grateful to the meticulous experimental support provided by Messrs. T. Dorrell, B. H. Gumbert, W. D. Kendzulak, and J. Z. Pawlowski. Mr. Pawlowski deserves particular thanks for all fabrication studies reported here.

Sincere thanks to Professor A. B. Metzner of the Department of Chemical Engineering, University of Delaware, for the many helpful discussions, constructive criticisms, comments, and suggestions on this work.

References

1. D. E. James, Paper presented at the 11th CDC International Business Conference, Brussels, Belgium, April 11–18, 1985.
2. J. C. Miller and S. J. Kurtz, Paper presented at the IX International Congress on Rheology, October 8, 1984.
3. C. J. S. Petrie and M. M. Denn, *AIChE J.*, **22**, 209–236 (1976).

4. S. Middleman, *Fundamentals of Polymer Processing*, McGraw-Hill, Inc., New York (1977), p 475.
5. J. P. Tordella, *J. Appl. Polym. Sci.*, **7**, 215–229 (1963).
6. A. P. Metzger and C. W. Hamilton, *S.P.E. Trans.*, **4**, 107–112 (1964).
7. J. J. Benbow and P. Lamb, *S.P.E. Trans.* (Jan. 1963).
8. J. P. Tordella, In *Rheology*, Vol. 5, F. R. Eirich, ed., Academic Press, New York (1969).
9. P. L. Clegg, In *The Rheology of Elastomers*, P. Mason and N. Wookey, eds., Pergamon Press, New York (1958), p 174. Also see: *Trans. J. Plas. Inst.*, 28, 245 (1960).
10. C. L. Sieglaff, *S.P.E. Trans.*, **4**, 129 (1964).
11. J. M. Lupton and R. W. Register, *Polym. Engr. Sci.*, **5**, 235 (1965).
12. A. B. Metzner, E. L. Carley, and I. K. Park, *Mod. Plas.*, 133 (July 1960).
13. E. B. Bagley, *Trans. Soc. Rheol.*, **5**, 355–368 (1961).
14. A. V. Ramamurthy, U.S. Patent 4,552,712 (1985).
15. A. V. Ramamurthy, U.S. Patent 4,554,120 (1985).
16. A. V. Ramamurthy, U.S. Patent 4,522,776 (1985).
17. S. S. Schwartz and S. H. Goodman, *Plastic Materials and Processes*, Van Nostrand Reinhold Co., New York (1982).
18. Barex 210 Technical Literature, Vistron Corp., Cleveland, Ohio.
19. P. S. Blatz, U.S. Patent 3,125,547 (1964).

Received September 9, 1985
Accepted November 22, 1985

35

eriment. Thus, the flow
well-defined rheological

elt indexer" is a useful
ever, in comparing res-
note that two materials
have viscosity curves of
e 4-13.
he test exactly the same
is defined only in terms
rimental procedure, the
ervations made using a
devices. If a quantity of
a melt indexer can be

terize molten polymers,
's the Rossi-Peakes flow
est method D569-59**:
tic molding compounds."

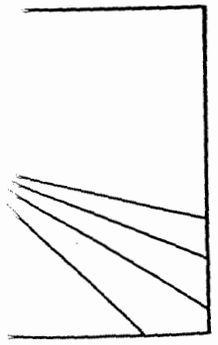

ESS

having the same melt index.

thod 105A).

A premolded, cylindrical specimen is placed at room temperature in a "charge chamber" (barrel) at the bottom of a steam-heated block which also contains a capillary with a diameter of 0.125 inch and a length of 1.5 inches. A piston is immediately raised into position and presses against the polymer, causing it to flow upward into the capillary. A specified upward driving pressure is supplied by means of weights suspended from pulleys. The rate of rise of polymer in the capillary is monitored by means of a follower rod which rests on the surface of the melt. The quantity reported is the temperature at which the flow in the first 2 minutes is 1 inch.

If polymer were preheated and allowed to fill the capillary, the Rossi-Peakes flow tester could be used as a crude capillary viscometer. In this case, it would be subject to most of the same sources of inaccuracy as the melt indexer, although the standard capillary for the Rossi-Peakes test has a much larger L/D. However, when used as specified in ASTM D569-59, this device yields a reading which depends not only on an unknown combination of rheological properties, but also on its melting and heat transfer characteristics. It is not intended to measure a material property, but to simulate, in some sense, the molding process.

A commercial version of the Rossi-Peakes tester is described in Section 9.3.

Maxwell and Jung [85] designed a weight-driven capillary rheometer for the study of the effect of pressure on melt viscosity. Like the Westover instrument described in the next section, it has barrel sections on both sides of the capillary, and both are fitted with pistons. A hydraulic hand pump, acting on the upper piston, supplies the elevated static pressure, while the driving pressure is applied to the lower piston by means of dead weight loading. This rheometer is simple, compact and portable.

4.4.2 Use of Compressed Gas to Drive Capillary Flow

Weight-driven capillary rheometers are, for practical reasons, limited to moderate driving pressures and thus to rather low shear rates. They therefore supply information only about the lower end of the viscosity curve and are of little value in distinguishing between resins whose viscosity curves are different in shape. This was recognized by Bagley and others working in the CIL laboratories,* and Bagley [53] has described the rheometer they developed as a result. In this device, which has come

*Canadian Industries Limited, Montreal.

to be called the "CIL high shear viscometer," the driving pressure is applied by means of pressurized nitrogen. Figure 4-14 shows the basic features of the instrument. The polymer (2) is heated by an electrical heater (4), and its temperature is monitored by two thermocouples (5). Nitrogen pressure is applied through a hose (7) and the melt flows through the die (1). To ensure an even flow of melt in the barrel, a steel ball (3), slightly smaller than the barrel, is used to transmit the gas pressure to the melt.

This instrument has been used in a number of important studies of

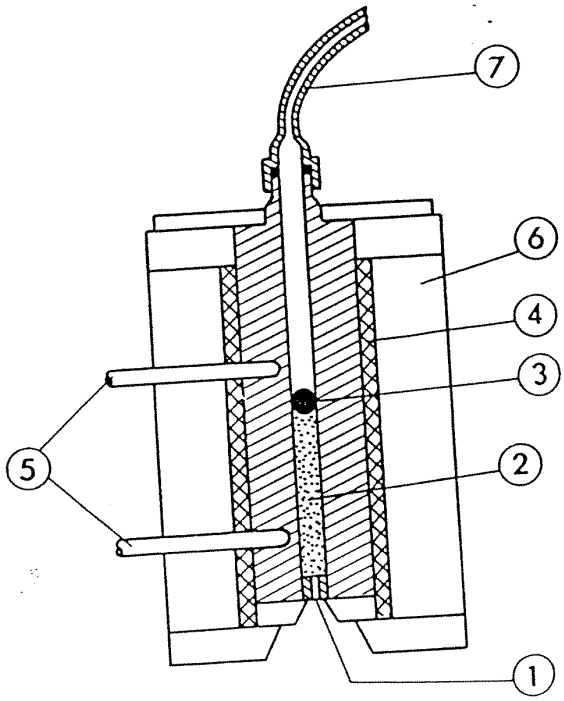

Figure 4-14. Essential elements of Bagley's rheometer [53]. (Reproduced from J. L. Leblanc [16] with the permission of Editions CEBEDOC, Liege.)

ymer melt flow and also as a quality control tester. A widely used ndard test involves the use of the following die geometry and oper- ng conditions.

Die diameter = 0.01925 inch
Die length = 0.1760 inch
Pressure = 1,500 psia
Temperature = 190°C

The flow rate is determined by weighing the polymer extruded in a fixed length of time and, for these particular conditions, the extrusion rate in grams/10 minutes is called the "CIL flow index."

Benbow and Lamb [86] designed a miniature version of the CIL viscometer for use with very small samples.

It has been reported that it is sometimes difficult to achieve steady flow in the CIL-type instrument. Schreiber [87] measured the flow rate as a continuous function of time and found that periods of 30 to 60 minutes were often required to achieve a constant flow rate. In some cases, no steady state was obtained even after one hour. Furthermore, Schreiber and Rudin [84] found that a sudden increase in pressure during extrusion actually decreased the flow rate of low density polyethylene. These observations demonstrate that a constant gas pressure does not necessarily lead to a constant flow rate, so that the existence of a steady state must be verified by flow measurements over several time periods.

For viscosity measurement at high shear rates, the CIL type viscometer has been largely replaced by rheometers with servohydraulic and electromechanical drive systems, in spite of their much greater complexity and cost. However, three commercial versions that are still available are described in Chapter 9.

Ramsteiner [88] has developed a pressure-driven capillary device that allows one to monitor with high precision the flow rate as a function of time. Gas pressure in the barrel forces the polymer through the die into an oil bath, which is heated electrically. The volume of oil displaced by the molten extrudate is measured electronically. A viewing port in the oil bath allows for observation of the behavior of the extrudate so that this device is useful for the study of isothermal extrudate swell and flow instabilities.

Another method for transmitting gas pressure to the melt in the bar-

36

Correlation of Low Density Polyethylene Rheological Measurements with Optical and Processing Properties

M. SHIDA, R. N. SHROFF, *and* L. V. CANCIO*

Chemplex Company
Rolling Meadows, Illinois 60008

The processing properties of low density polyethylene melts, such as drawdown and neck-in, and the final product properties, such as film haze and gloss, have been successfully correlated with rheological functions and the level of long-chain branching. The rheological functions employed are the entrance pressure drop ΔP_e and the swell ratio S_e, determined at a specified shear stress using an orifice with a length/diameter (L/D) ratio of zero. The calculation of shear stress requires additional measurements using a die with a finite L/D e.g. 20. The rheological functions ΔP_e and S_e are governed by the level of high molecular weight species and/or the level of long-chain branching (LCB). If determined at a constant shear stress, in order to eliminate the effect of viscosity, they are a relative measure of elasticity. Higher ΔP_e and S_e indicate a higher level of LCB and correlate with poorer optical properties and drawdown in films.

INTRODUCTION

Our previous study (1) involved the successful prediction of the processibility of high density polyethylenes from capillary flow steady-flow viscosity vs shear rate data in the shear rate range of approximately 1-600 sec^{-1}. Such data were curve-fitted to the empirical equation of Sabia (2):

$$\ln (\eta/\eta_o) = (\eta/\eta_o - a) \ln (1 + (\dot{\gamma}\tau_c)^b) \qquad (1)$$

where $ab = 2/3$, a is the adjustable parameter and η_o (limiting viscosity at low shear) and τ_c (maximum relaxation time) are obtained as shift factors in the least squares analysis of the linear form of *Eq 1* through an iterative procedure using a computer. The limiting viscosity at low shear, η_o, generally agreed well with values measured using a Weissenberg rheogoniometer (WRG) for a number of high density polyethylenes. Also emerging from such a curve fitting procedure is the processibility parameter R_D defined by the relation (1):

$$R_D = C\ (\tau_o^{0.75}/\eta_o) \qquad (2)$$

where C is an arbitrarily selected constant chosen to yield numerical value for R_D of between 1 and 20.

We were, however, not successful in applying *Eq 1* to many of the low density or the branched polyethylenes studied here. The reasons are twofold. First, η_o obtained from the curve fitting procedure does not agree with the measured η_o from WRG. Second, the viscosity-shear rate data in the $\dot{\gamma}$ range of 1-600 sec^{-1} are not necessarily different for resins differing greatly in their molecular weight distribution (MWD) or the level of long-chain branching. Specifically, R_D may not differ significantly among various resins even though the MWD at the high molecular weight end varies greatly.

Since the viscous response at the higher shear rates does not reflect the change in the high MW portion of the MWD curve, we have shifted our emphasis to the measurements of elasticity in an effort to relate the latter to some of the processing and the product properties of the low density polyethylenes. The reason is that optical and drawdown properties of branched polyethylenes are governed by the presence or lack of high MW species. The elasticity functions of interest are the entrance pressure drop ΔP_e and swell S_e measured using capillary rheometer with an orifice having a length/diameter (L/D) ratio of zero.

EXPERIMENTAL

A number of commercially available low density or branched polyethylene (LDPE) resins, ranging in melt index (MI) from 0.2-13, were used in this study.

The molecular weight distribution was obtained on a Waters Associates gel permeation chromatograph (GPC) Model 200 with a series arrangement of four columns of porosity rating from 2.5×10^3 Å to 5×10^6 Å. 1, 2, 4-trichlorobenzene was used as the solvent at 135°C. The flow rate was 1 ml/min, injection time was 2 min, and the sample weight was 0.5 g (diluted to 200 ml). The long-chain branching (LCB) level was derived using combined GPC and intrinsic viscosity measurements in TCB at 135°C.

Steady state flow data in the shear rate range of 0.006-2 sec^{-1} were obtained on a Weissenberg rheogoniometer

* Present address: Chemplex Corp., Cincinnati, Ohio 45246

at 190°C using 2.5 cm diameter platens. At shear rates for 4-1000 sec^{-1}, the data were obtained from a gas extrusion rheometer at 190°C using two dies. One was of 0.043 in. diameter (D) and had a 90° entrance angle with an L/D of 20. The other was an orifice ($L/D = 0$) with a 90° entry angle and $D = 0.060$ in. Both Rabinowitsch and entrance corrections (3) were applied in the usual way to determine the true shear rate and the true shear stress at the capillary wall, respectively. A gas extrusion rheometer was used in preference to the Instron rheometer because the entrance pressure drop and the swell ratio measured using the orifice involve pressures as low as 5 psi. The rheometer was equipped with 0-100 psi gauge with an accuracy of ±0.1 percent of full scale. In this rheometer, volumetric flow rates Q and swell cuts were measured at preselected pressures, yielding the true shear stress τ and the true shear rate $\dot{\gamma}$ from the relations: $\tau = (\Delta P - \Delta P_a)/4(L/D)$ and $\dot{\gamma} = (32Q/\pi D^3)[(3n + 1)/4n]$, where n is the slope of apparent shear stress vs apparent shear rate curve. Here, ΔP is the pressure drop corresponding to a die with $L/D = 20$, and ΔP_a is the pressure drop at the same shear rate in the $L/D = 0$ orifice.

Along with ΔP_a measured directly using the orifice, we also measured S_a, defined as the ratio of an unannealed extrudate sample diameter to the orifice diameter. For the purpose of this article, we did not find it necessary to anneal the swell extrudates (4, 5).

Percent haze is defined as the percentage of transmitted light scattered by the film more than 2.5° from the normal incident beam and was measured according to ASTM D-1003 using a Gardner pivotable sphere hazemeter.

Films were made using a blow film process using a 3.5 in. extruder of 24:1 L/D which was equipped with an 8 in. side fed die. The die gap was set at 0.025 in. and film with nominal gauge of 0.001 in. was produced at 150 pounds per hr at a blow up ratio of 2:1.

RESULTS AND DISCUSSION

Melt index (MI) and density (ρ) are the most widely used parameters by which various branched polyethylene resin grades are described. While MI provides a relative measure of molecular weight and viscosity level, it ignores the non-Newtonian nature of flow and does not account for the differences in molecular weight distribution (MWD) and long-chain branching. For example, two resins used in extrusion coating and casting applications have flow curves with different low shear viscosities but the same viscosities at shear rates greater than about 2 sec^{-1} (*Fig. 1*) even though the apparent molecular weight distributions are widely different (*Fig. 2*). As may be inferred from the intercept with the line in *Fig. 1* giving the value of the melt index shear stress, the melt indices, measured at $\dot{\gamma} > 2$, are the same (MI ≃ 3.3). In *Fig. 2* and other figures showing MWD, the normalized curve height is plotted against elution count, which is inversely related to logarithmic molecular weight. The MWD curves are not corrected for long-chain branching and are shown as raw chromatograms for the sake of convenience.

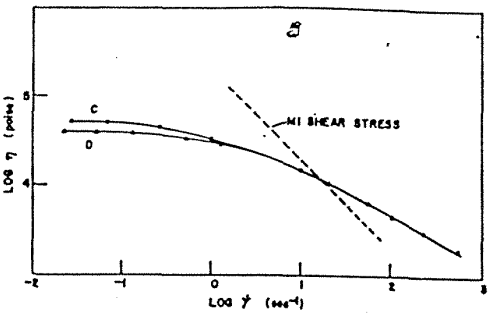

Fig. 1. Viscosity plotted against shear rate for two branched polyethylenes, C and D, at 190°C. The value of the shear stress used in the MI measurement is represented by the dashed line.

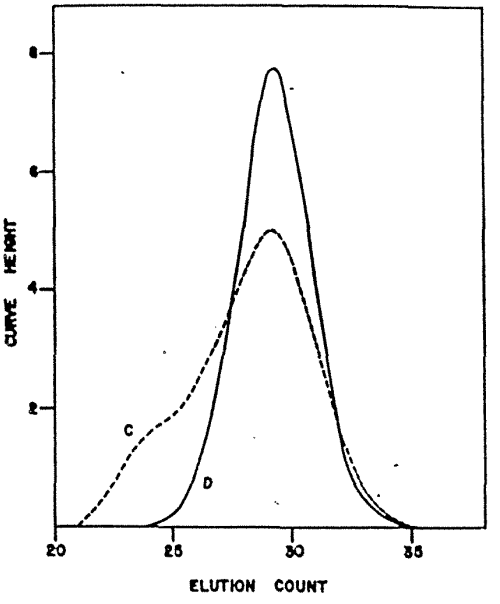

Fig. 2. Normalized GPC chromatographs showing apparent molecular weight distribution in the form of curve height vs elution count for two branched polyethylenes, C and D, of MI 3.3.

From the data in *Figs. 1* and *2*, it is noticed that the great difference in the high MW portion, or the level of LCB, is not reflected in the viscous response at $\dot{\gamma} > 2$ sec^{-1}. Thus, R_D for resins C and D in *Fig. 1* is the same. However, a difference in the viscous response at $\dot{\gamma} > 2$ sec^{-1} does exist if there is a significant difference in the lower MW end of the GPC distribution curve. For example, two LDPE molding grade resins have the same MI and density but differing level of lower MW species (*Fig. 3*) and show a significant difference in R_D (*Fig. 4*).

For the majority of low density resins studied here, however, some of the processibility and product properties are influenced by the level of LCB or the level of

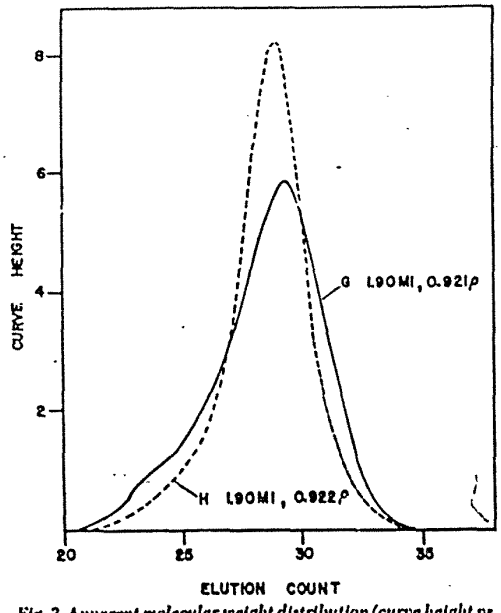

Fig. 3. Apparent molecular weight distribution (curve height vs elution count) for branched polyethylenes G and H, both of MI 1.9.

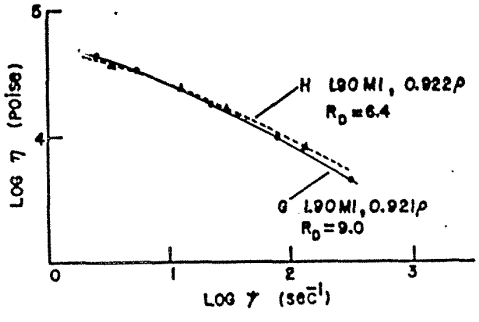

Fig. 4. Viscosity plotted against shear rate for two branched polyethylene resins, G and H, at 190°C.

higher MW species (6). We will not consider here the effect of a difference in the low molecular weight species on the rheological functions. It is difficult to make a true distinction between LCB and high MW species because, in the free radical process of LDPE polymerization, one accompanies the other. Therefore, in view of the concept of a shear rate-dependent relaxation spectrum, (7), it would be reasonable to expect that the flow properties of importance for such LDPE resins should be those obtained at low shear rates, such as the steady-flow viscosity η and the first normal stress difference ($P_{11} - P_{22}$)—both measured at low shear rates using the WRG. The transient shear stress and normal stress measurements in the WRG would perhaps be even more sensitive than the steady state measurements in detecting such a change in LCB level and hence the resulting change in the product properties and the processing behavior.

Unfortunately, such measurements are time consuming, relatively inaccurate and, therefore, not suitable for rapid resin characterization. The solution to this problem emerged from the following two considerations: (a) the entrance pressure drop ΔP_e is reported to be related (8) to the first normal stress difference and other elasticity functions such as the exit pressure (9) and the die swell ratio, and (b) we have used (10) a technique of measuring ΔP_e directly using an orifice (die with L/D = 0), thus avoiding time consuming Bagley plots (3). A further advantage from a practical standpoint for using ΔP_e and S_e is that these functions represent the result of a tensile or elongational deformation superimposed on a shear deformation, deformations that exist in all processing operations (11).

Since we are interested in relating ΔP and S_e to the LCB level, and they in turn correlate with the optical and the drawdown properties of branched polyethylenes, we will briefly review how the LCB level, as represented by the weight average number of branch points per molecule, n_w, is obtained. It is derived from combined GPC-intrinsic viscosity data (12) using the following relation:

$$(\eta)_H = (\eta)_l\, g^{1.5} = KM^a\, g^{1.5} \qquad (3)$$

where $(\eta)_l$ and $(\eta)_H$ are the intrinsic viscosities for the linear and branched polyethylene of the same molecular weight, and K and a are the constants in the Mark Houwink equation. The g factor in *Eq (3)* is related to the number of branch points per molecules, n, by the equation:

$$g = [(1 + n/7)^{\frac{1}{2}} + 4n/9\pi)^{-\frac{1}{2}}$$

$$m = (\lambda M/2)\,[I_3\,(\lambda M)/I_2(\lambda M)]$$

where I_2 and I_3 are the modified Bessel functions of order 2 and 3, respectively. An iterative procedure is used by assuming an initial value of λ (unknown) until the calculated $(\eta)_B$ agrees with the measured value. Because of the non-linear dependence of λ on the molecular weight, the relation $n_w = \lambda M_w$ does not hold, although as a first approximation $n_w \simeq \lambda M_w$. The details of this calculation appear in an earlier publication (12).

An illustration of the influence of n_w on ΔP_e and S_e is shown in *Fig. 5* for the two resins whose apparent MWD appears in *Fig. 1*. Note that both resins C and D have the same melt in *Fig. 1*. Note that both resins C and D have the same melt index, but resin C, with a high n_w of 56, has significantly higher ΔP_e and S_e at a given shear rate than does resin D (*Fig. 5*), where n_w = 9. While the resins C and D are chosen for illustrative purpose, one seldom uses in commercial practice two widely dissimilar resins for the same application. One is thus interested in detecting small differences in the LCB level for resins with roughly the same MWD and MI and relating these differences to such product properties as haze and gloss and to a processing parameter such as drawdown.

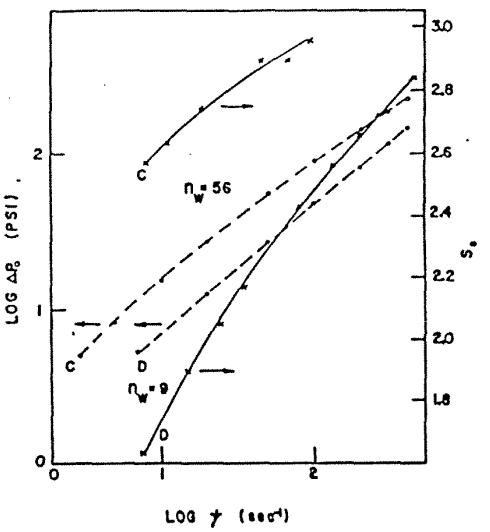

Fig. 5. Entrance pressure drop ΔP_0 and swell ratio S_0 vs shear rate for branched polyethylene resins, C and D, having differing long-chain branching levels η_w. Data at 190°C.

However, the functions ΔP_0 and S_0 for a set of resins are dependent on MI or viscosity level even if the MWD or LCB level is the same. ΔP_0 and S_0 at a given shear rate are higher if the melt index is lower. This is illustrated in *Fig. 6* for three low density resins with more or less similar MWD. In order to eliminate the melt index or the viscosity variation effect, the same two functions are used at constant shear stress τ instead of at constant shear rate $\dot{\gamma}$. ΔP_0 and τ_0 at a given shear stress reflect the elasticity of resins even if the viscosity is different.

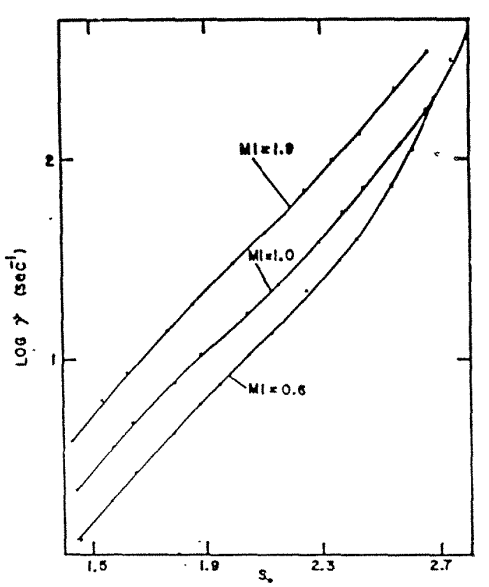

Fig. 6. Shear rate vs swell ratio (S_0) from an orifice for three branched polyethylene resins of differing melt index.

From the data in *Fig. 6* and our experience, it is observed that for many branched polyethylenes, both ΔP_0 and S_0 become less sensitive to LCB level or η_w as one goes to higher $\dot{\gamma}$ or higher τ. Therefore, ΔP_0 and S_0 at the lowest common τ are used to correlate several resins with respect to their optical properties or drawdown behavior. It may be noted that the resins designated by codes C, D, G and H and shown in *Figs. 2-5* are used only to illustrate how a large difference in LCB level affects the viscosity and the elasticity of the resins and hence the optical properties. For example, percent haze for film from resin type C is 17, whereas it is 6.0 for resin type D. Our discussion below, on the other hand, will be confined to resins whose "gross" behavior is the same but where finer differences need to be distinguished.

Haze for Clarity Resins

The resins used in a clarity film application all had a nominal melt index of 1.5 and a density of 0.922 g/cm³. The lowest common τ for these resins is 2.8×10^5 dynes/cm², which corresponds to data measurement in the vicinity of 17 psi for the orifice.

The general purpose clarity film grade resins considered here all have the MWD of the type shown for resin D in *Fig. 1*. We will now consider what factors govern the optical properties of the film produced by a blown film process.

Huck and Clegg (13) have pointed out that if the density of the resin is below 0.925 g/cm³, extrusion defects are the predominant contributor to the total haze of the film. For higher density resins, crystallization defects can be quite significant and contribute considerably to the total haze. Extrusion defects in low density blown films are predominantly caused by higher melt elasticity and a higher level of LCB. Therefore, haze increases with increase in elasticity as measured by ΔP_0 (*Fig. 7*) and S_0 (*Fig. 8*) and an increase in LCB as reflected by an increase in the level of high MW species (*Fig. 9*). It may be remarked here that the difference in the high MW portion of the GPC curves as seen in *Fig. 9* is reproducible but small, whereas the same three resins show a large difference in the rheological parameters ΔP_0 and S_0 (*Figs. 7-8*). It may also be noted that if the internal haze contribution to the total haze is large, as when the film is thick and/or if the resin density is high, then ΔP_0 and S_0 may preferably be correlated with another optical property parameter, gloss, which depends only on the surface irregularity.

Drawdown for Liner Resins

Resins for use in a liner film application had a nominal melt index of 3.0, and the lowest common τ for these resins was 1.1×10^5 dynes/cm², corresponding roughly to the data taken at 7 psi in an orifice.

The liner film resins considered here all have the MWD of the type shown for resin C in *Fig. 1*, although the extent of such a high level of LCB may be reduced depending on how the resin is manufactured.

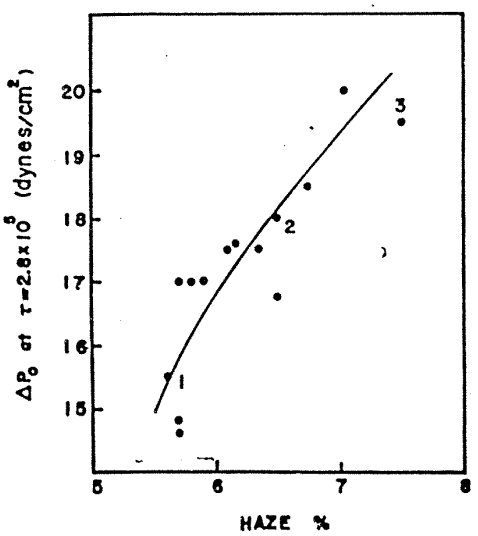

Fig. 7. Entrance pressure drop at a constant shear stress plotted against haze for branched polyethylene resins used in clarity film application.

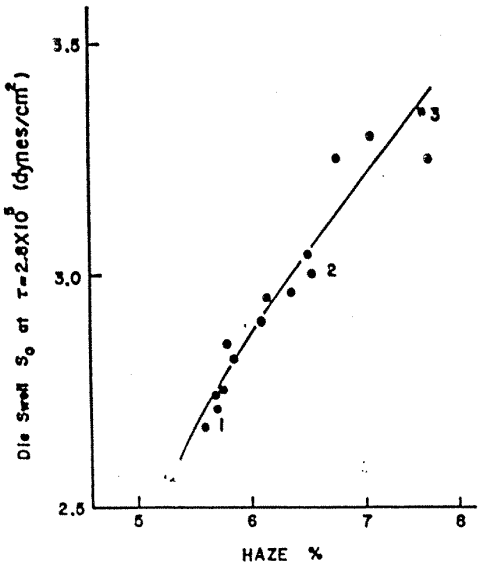

Fig. 8. Swell ratio at a constant shear stress plotted against haze for branched polyethylene resins used in liner film application.

Factors very similar to those affecting the optical properties of a film apply to the ease with which LDPE melt can be drawn down to give a thin film or coating. Ease of drawdown depends on both the viscosity and the elasticity of the melt. Accordingly, low MW (high MI), low elasticity, and a low level of long-chain branching are preferred. For resins with a higher MI, such as those considered here for linear resin applications, the swell

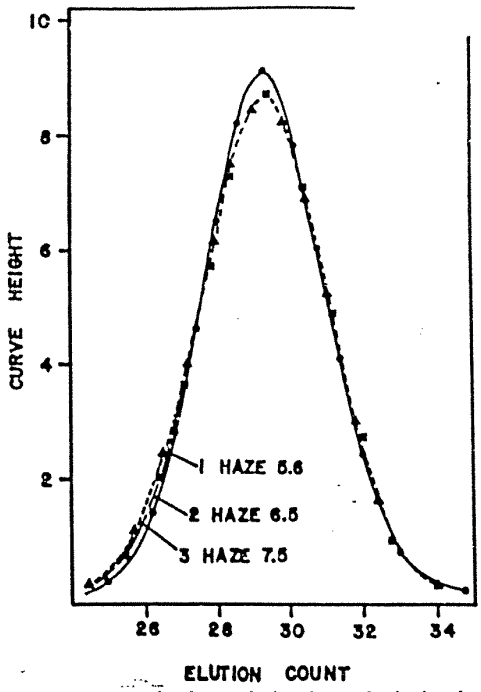

Fig. 9. Apparent molecular weight distribution for the three low density polyethylenes designated 1, 2, and 3 in Figs. 7 and 8.

values could not be reliably measured because of the sagging of the extrudate as it emerged from the orifice. Therefore, ΔP_e at constant τ was used as a measure of elasticity and LCB level in order to characterize drawdown performance. As can be seen from the data in *Table 1*, ΔP_e at a given τ correlates well with behavior in the field.

CONCLUSIONS AND SIGNIFICANCE

We have shown how capillary rheometry, using an orifice die, i.e., a die whose length/diameter ratio is zero, yields rheological elasticity functions which relate to the level of long-chain branching in low density polyethylene. Such functions are the entrance pressure drop ΔP_e and swell S_e at a specified shear stress. The usefulness of these functions is illustrated by the correla-

Table 1. Drawdown Behavior

Resin	MI	Field experience	ΔP_e at τ = 1.1 × 10⁵ dynes/cm²
1	3.3	Good—Customer A	4.5
2	3.3	Good—Customer B	4.9
3	3.0	Good—Chemplex	5.2
4	3.2	Good—Customer C	5.7
5	3.5	Borderline/bad—Customer C	6.0
6	3.4	Bad—Customer A	6.2
7	2.7	Bad—Customer D	6.9
8	3.1	Bad—Customer C	7.7
9	2.7	Bad—Customer E	7.7

tion of changes in the film optical properties of a series of commercial film grade resins with changes in S_o. For resins with higher MI, where swell of the extrudates is difficult to measure because of sagging, the drawdown performance or the ability of the film to be drawn down to thin gauge is successfully correlated with ΔP_o. This study illustrates the application of fundamental rheological principles to the optimization of resin processibility and physical properties.

REFERENCES

1. M. Shida and L. V. Cancio, *Polym. Eng. Sci.*, 11, 124 (1971).
2. R. Sabia, *J. Appl. Polym. Sci.*, 7, 347 (1963).
3. E. B. Bagley, *J. Appl. Phys.*, 28, 624 (1957).
4. N. Nakajima and M. Shida, *Trans. Soc. Rheol.*, 10, 299 (1966).
5. R. C. Kowalski, "Elastic Behavior in Molten Viscoelastic Polymeric Materials," Ph.D. dissertation, Polytechnic Institute of Brooklyn (1963).
6. E. J. Kaltenbacher, J. K. Lund, and R. A. Mendelson, *SPE J.*, 23, 55 (Nov. 1967).
7. R. N. Shroff and M. Shida, *J. Polym. Sci.*, C35, 153 (1971).
8. H. L. LaNieve and D. C. Bogue, *J. Appl. Polym. Sci.*, 12, 353 (1968).
9. C. D. Han, M. Charles, and W. Philippoff, *Trans. Soc. Rheol.*, 14, 393 (1970).
10. R. N. Shroff, M. Shida, and T. M. Krigas, *34th SPE Antec*, 411 (1970).
11. F. N. Cogswell, *Polym. Eng. Sci.*, 12, 64 (1972).
12. J. A. Cote and M. Shida, *J. Appl. Polym. Sci.*, 14, 3083 (1970).
13. N. D. Huck and P. L. Clegg, *SPE Antec, Tech. Papers*, 1, (1961).

JMS—REV. MACROMOL. CHEM. PHYS., C29(2 & 3), 201-317 (1)

37

A Review of High Resolution Liquid ^{13}Carbon Nuclear Magnetic Resonance Characterizations of Ethylene-Based Polymers

JAMES C. RANDALL
Baytown Polymers Center
Exxon Chemical Company
Baytown, Texas 77522

I. INTRODUCTION 202
II. EXPERIMENTAL 218
III. NOMENCLATURE 225
IV. ASSIGNMENTS 229
V. ETHYLENE–PROPYLENE COPOLYMERS 237
VI. ETHYLENE–1-BUTENE COPOLYMERS 256
VII. ETHYLENE–1-HEXENE COPOLYMERS 267
VIII. ETHYLENE–1-OCTENE COPOLYMERS 278
IX. LONG-CHAIN BRANCHING IN POLYETHYLENE . . 285
X. LOW-DENSITY POLYETHYLENE 297
XI. ETHYLENE–VINYL ACETATE COPOLYMERS 303
XII. CONCLUSION 312
REFERENCES 313

Copyright © 1989 by Marcel Dekker, Inc.

CANTECH
EXHIBIT
57
Interf. No. 103,404

Case 1:05-cv-00737-JJF Document 160-5 Filed 09/03/2008 Page 18 of 42

EXHIBIT PAGE 000993

I. INTRODUCTION

The use of ^{13}carbon nuclear magnetic resonance (NMR) spectroscopy in the molecular characterization of macromolecules has advanced our knowledge into structural areas that have been nearly impossible to measure by other spectroscopic techniques. Innovative applications have led to determinations of polymer configurational distributions, comonomer sequence distributions, average sequence lengths, structure and distribution of short chain branches, and analyses of nonreactive end groups. As a result, the importance of ^{13}C NMR to the field of polymer science cannot be overemphasized. The key to the success of ^{13}C-NMR studies in defining polymer molecular structure has been a structural sensitivity which encompasses more than just a few functional groups or carbon atoms. A sensitivity to polymer repeat unit sequences of lengths from two to as many as five, seven, and even nine contiguous repeat units [1, 2] has been observed. Of course, any structural technique that senses a unique response from as few as two successive repeat units will lead to a measurement of average sequence lengths [1, 3] and run numbers [4]. In addition to this excellent structural sensitivity, there has been an enormous improvement in the quantitative sensitivity of ^{13}C NMR in recent years. Detection of long-chain branching in polyethylene can now be made at a level of one per ten thousand carbon atoms [5], and newer generations of high field, higher sensitivity NMR spectrometers promise to extend this detection limit another order of magnitude.

It would be instructive at this point in this discussion to review some of the attributes that have made ^{13}C NMR so amenable to polymer structural analyses. For the sake of brevity, it will be assumed that the reader is basically familiar with the phenomenological descriptions of both ^{1}H and ^{13}C NMR. (It is a primary objective of this article to discuss the framework through which ^{13}C-NMR spectral information is transferred to useful polymer structural information, consequently very little time will be spent in phenomenological descriptions that are not required for an understanding of this "transfer process.") A significant advantage of ^{13}C NMR over corresponding NMR studies of other nuclei is that the ^{13}C nucleus has a spin of 1/2 and occurs at a natural abundance of approximately 1%. This latter property precludes any appreciable complications

from ^{13}C internuclear interactions and the former ensures isotropic magnetic behavior. Thus, from a quantum mechanical standpoint, ^{13}C NMR can be treated in a similar way to ^{1}H NMR. The carbon NMR spectral response to polymer structure is so sensitive to small changes that higher levels of ^{13}C isotopes would lead to hopelessly complex NMR spectral patterns, as encountered historically in corresponding ^{1}H-NMR studies of various homopolymers and copolymers [2]. Some isotopic ^{13}C labeling has been useful in certain polymers studies [6, 7]; however, the strength of the ^{13}C-NMR technique arises from the fact that ^{13}C nuclei are located in a sea of magnetically inactive ^{12}C nuclei and protons. The latter, although magnetically active, can be broad band noise decoupled cleanly and efficiently to remove all ^{13}C, ^{1}H interactions. The resulting spectra contain only single lines, each of which can be related to a specific carbon structural environment.

This part of the discussion leads us to the second major advantage of ^{13}C NMR of polymers, which is the wide range covered by ^{13}C chemical shifts. Expressed in ppm, the chemical shift is field independent and is defined by the frequency difference in hertz between an observed resonance and that of an internal standard divided by the ^{13}C-NMR resonance frequency (in MHz) as specified by the operating magnetic field. Typically ^{13}C NMR covers a chemical shift range of over 200 ppm, which is 20 times that usually encountered in ^{1}H NMR. In polymer spectra, this characteristic leads to well-delineated responses from the structural building units making up a polymer molecule.

The internal standard most often used in high-temperature NMR studies of polymers in solution is hexamethyldisiloxane (HMDS). Tetramethylsilane (TMS) is still the NMR chemical shift standard of choice but its low boiling point frequently precludes its use in NMR studies of polymers. It is preferable to report all polymer chemical shifts with respect to tetramethylsilane (TMS) by correcting the HMDS chemical shifts to a TMS standard. The chemical shift difference between TMS and HMDS is approximately 2.0 ppm, but the precise difference should be established independently on each spectrometer.

The final attributes contributing to the success of ^{13}C NMR polymer structural analyses are a result of significant advances

in instrument technology. Operation in the Fourier transform mode [8] has made high sensitivities possible and permits a trade-off between high sensitivity and resolution [8] whenever desirable. Sometimes the low natural abundance of the ^{13}C isotope is easily glossed over in view of the ease with which ^{13}C-NMR spectra are obtained on the commercial NMR instrumentation available today. Broad-band decoupling [9] not only removes all ^{1}H spin-spin coupling with ^{13}C nuclei but also results in the creation of the nuclear Overhauser effect (NOE), a phenomenon that occurs only during broad-band decoupling and leads to enhancements in resonance intensities independently of the population of contributing nuclei. The magnitude of the nuclear Overhauser effect can be variable and is related to the specific mechanisms through which nuclear spins relax after excitement by a radiofrequency field. Fortunately for most polymers, the nuclear Overhauser effect is more an asset than a liability because of the restricted mobility of polymers [9], which leads to the dipole-dipole relaxation mechanism as the principal, if not the only, mode of nuclear relaxation. The nuclear Overhauser effect operates exclusively through the dipole-dipole relaxation mechanism, consequently most polymers exhibit the maximum NOE effect of 3.0 [9] and desirable quantitative analyses go unimpeded. If there is any question of differences among NOE's in polymer NMR spectra, gated decoupling experiments can be performed to ensure equal NOE's throughout the NMR spectrum [8]. These factors, together with a patient accumulation of data through time averaging, have led to quantitative measurements of concentration levels of one carbon type per 10,000 total carbon atoms, as mentioned earlier. It is this combination of good spectral sensitivity to low concentration levels in conjunction with excellent structural sensitivities that has made ^{13}C NMR so valuable in polymer characterization.

With the advantages of ^{13}C NMR now briefly reviewed, it is appropriate at this point to discuss polymer structure in terms of a framework compatible with the information retrieved from ^{13}C-NMR analyses. "Polymer structure" can evoke a different response, depending upon the particular area of interest, from various polymer scientists. It can encompass morphological structures, properties, molecular weights, and even flow properties of polymer melts. Polymer structure in this discussion will refer to the actual molecular chain structure, that is, the identity of the repeat unit and its chirality, sequence structures and their distributions, the identity of end

groups including numbers and types per molecule, the degree of polymerization, and the identification of both short- and long-chain branching. For homopolymers, the interest in polymer molecular structure is limited to the degree of polymerization, chirality and variation in modes of monomer additions, the identity of end groups, and extent of long-chain branching. Copolymer structural analyses encompass all of the factors encountered in analyses of homopolymers but with additional complications arising from various possible sequence distributions. Homopolymers with one pendant group per repeat unit can often be treated as copolymers because of chiral differences that may arise within repeat unit sequences. Mathematically, sequence distributions are treated in the same way whether they arise from chiral differences or differences in repeat unit structures created by using different comonomers during polymerization. Because polymer chirality is inherently included in A,B copolymer descriptions and has been well covered independently previously [2, 3], the development of structural concepts and characterization parameters in the upcoming discussion will be limited to A,B types of copolymers. The mathematical treatment is, therefore, quite general but will be applied exclusively to ethylene-based polymers, that is, low-density polyethylene, linear low-density polyethylenes, and ethylene–vinyl acetate copolymers, which are also produced free radically in a high-pressure process.

Prior to the advent of ^{13}C NMR, knowledge of repeat unit structure and the relative A,B concentrations for copolymers was usually all that could be determined from a micromolecular structural viewpoint. Endgroup concentrations could be measured for many step-growth polymers if the polymer chain ended in a functional group that was active chemically, but aliphatic end groups from chain-growth polymers usually went uncharacterized. Repeat unit structures of both chain-growth and step-growth polymers were often determined by either infrared or ^{1}H NMR. The missing ingredient in most copolymer analyses was the concentration of unlike contiguous pairs of polymer repeat units, that is, the AB+BA diad concentration. Any polymer chain, whether a homopolymer or copolymer, can be visualized as being derived from any one or all of the three exclusive types of diads, that is, AA, AB+BA, or BB. Knowledge of the three diad concentrations, whether absolute or relative, leads to the A,B mole fractions, average sequence lengths for both A and B, and the "run number," which is the number of runs collectively of both units per 100 contiguous repeat units, as defined by Harwood and Ritchey [4]. The

relationships among "n-ads," that is, diads, triads, tetrads, etc., and the various resulting derived structural parameters can best be understood by examining a model A,B copolymer chain where the sequence arrangements and number or runs, etc., can be easily viewed and counted.

The following A,B copolymer chain has a typical random copolymer sequence distribution. The ends are tied together for two reasons: first, to approximate a long chain, and second, to remove any discrepancies in the various *n*-ad distributions created by end groups. The advantage of depicting such a copolymer chain is that any derived algebraic structural relationships can be tested directly.

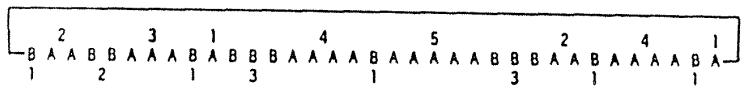

A "run is defined as an uninterrupted sequence of like repeat units and varies from unity to the longest sequence the chain will allow. In the above model chain, the length of each "A" run is given directly above each contiguous "A" sequence while the length of each "B" run is given directly below each contiguous "B" sequence. The "A" and "B" sequence distributions can be broken down as follows:

Run length (*i*)	Sequence	Number (A_i)	Sequence	Number (B_i)
1	BAB	2	ABA	5
2	BAAB	2	ABBA	1
3	BAAAB	1	ABBBA	2
4	BAAAAB	2	ABBBBA	0
5	BAAAAAB	1	ABBBBBA	0
6+	$B(A)_{6+}B$	0	$A(B)_{6+}A$	0
	ΣA_i	8	ΣB_i	8

where A_1 = #BAB sequences

A_2 = #BAAB sequences, etc.

and the corresponding definition goes for the "B" sequences.

The number of "A" sequences and the number of "B" sequences in the above model chain are, therefore, given by

$$\text{Number of "A" sequences} = \Sigma A_i \tag{1}$$

$$= 2 + 2 + 1 + 2 + 1 = 8$$

and

$$\text{Number of "B" sequences} = \Sigma B_i \tag{2}$$

$$= 5 + 1 + 2 = 8$$

In the above model, it should be noted that the total number of "A" sequences is the same as the total number of "B" sequences, which is a "necessary relationship" encountered in copolymer sequences distributions. That is,

$$\Sigma A_i = \Sigma B_i \tag{3}$$

Whenever the ends of the chain are connected conceptually, the number of "A" sequences will always equal the number of "B" sequences, which hereafter will be called the "sequence number." In practice, Eq. (3) will be valid for copolymers having high degrees of alternations between A and B sequences or a random distribution of "A" versus "B" chain ends. Otherwise the "A" sequence number can differ from the "B" sequence number by ±1, depending upon whether the chain terminates uniquely in "A" units or "B" units. This difference becomes important only when the number of A,B alternations is low. For random and alternating copolymers, the "A" and "B" sequence numbers will be the same. Consideration has to be given for block copolymers having only a few blocks per chain. For an ABA triblock copolymer, the "A" sequence number is 2 while the "B" sequence number is 1. If the ends of this triblock copolymer are connected conceptually, both sequence numbers become unity.

The total number of "A" repeat units and the total number of "B" repeat units can be defined from the above sequence distributions as follows:

$$A_{Tot} = \Sigma iA_i \qquad (4)$$

$$= 1(2) + 2(2) + 3(1) + 4(2) + 5(1) + 6+(0) = 22$$

and

$$B_{Tot} = \Sigma iB_i \qquad (5)$$

$$= 1(5) + 2(1) + 3(2) + 4(0) + 5(0) + 6+(0) = 13$$

The average "A" and "B" sequence lengths are given, respectively, by the number of "A" repeat units divided by the sequence number and the number of "B" repeat units divided by the sequence number:

$$\text{"A" average sequence length} = \Sigma iA_i / \Sigma A_i \qquad (6)$$

$$= 22/8 = 2.75$$

and

$$\text{"B" average sequence length} = \Sigma iB_i / \Sigma B_i \qquad (7)$$

$$= 13/8 = 1.625$$

Finally, the run number (4), which is the total number of "A" plus "B" sequences per 100 units, is given by

$$\text{Run number} = (\Sigma A_i + \Sigma B_i) \times (100/(A_{Tot} + B_{Tot})) \qquad (8)$$

$$= (8 + 8) \times 100/35 = 45.7$$

The "run number" is not as useful as the "sequence number," but does give the average number of times the repeat units

switch from A to B and back to A per 100 repeat units. The "sequence number" expressed per 100 units will always be one-half the run number, which is 22.85 in the above example. More will be given later regarding the relative value of run numbers versus sequence numbers. For the time being, it is important to see how sequence distributions can be utilized to generate much-needed structural information.

The above analysis depended upon observations of complete "A" and "B" sequence distributions over sequences of all possible "A" and "B" lengths. Such structural information is generally not available. It is possible from NMR to obtain a complete A,B sequence distribution within a finite sequence length. This latter distribution represents the total number of ways A and B can be combined within a specific given sequence length. The net result is an A,B diad, triad, or higher order *n*-ad distribution. As it turns out, this latter distribution can lead to the same structural information as the former distribution without knowing the length of the longest "A" or "B" sequence. In addition, similar structural information can be obtained from any complete "*n*-ad" distribution because the various *n* ad distributions are related through so called "necessary relationships" [3]. The characterization of the previous model chain will now be repeated, but this time more realistically in terms of quantitative information that is available experimentally from NMR. The model chain is repeated below with diads of repeat units identified. Each repeat unit is part of two diads by being the end unit of a previous diad and the beginning unit of the next diad. The AA and BB diads are identified above the chain while the AB and BA diads are identified below the chain:

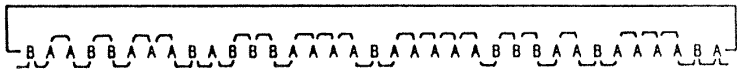

The numbers of diads of each type are

AA = 14

AB+BA = 16

BB = 5

First, it should be noted that the number of AB diads per chain must be the same as the number of BA diads per chain for copolymers with high degrees of A,B alternations or, as in the above example, when the end groups are tied together conceptually. Second, from a directional viewpoint experimentally, AB diads cannot usually be distinguished from BA diads because it is only in rare cases that the chain direction can be established. Consequently, these diads are counted together as AB+BA diads. Finally, the sum of the diads gives the total number of units in the copolymer chain. In this particular example, there is a total of 35 repeat units. The total numbers of "A" or "B" units, respectively, can be determined from the diad distribution as follows:

$$A_{Tot} = A = \Sigma iA_i$$

$$= (2AA + AB + BA)/2 = AA + 1/2(AB+BA) \quad (9)$$

$$= 22$$

and

$$B_{Tot} = B = \Sigma iB_i = BB + 1/2(AB+BA) = 13 \quad (10)$$

Equations (9) and (10) define the first of the necessary relationships between "monads" and diads. Other relationships will be developed shortly, and a complete list of "necessary relationships" up to pentads is given in Table 1. The run number and sequence numbers can be determined from the diad distribution because each "A" run begins with a BA and ends with an AB irrespective of the "A" sequence length. The "B" runs are counted in the reverse way since all "B" runs begin with AB and end with BA. Consequently, the run number is given by

$$\text{Run number} = (AB + BA) \times 100/(A+B) \quad (11)$$

which is

$$= (16) \times 100/35 = 45.7$$

in the model chain.

TABLE 1

The Necessary Relationships among Relative Concentrations of All Possible Sequence Combinations from Monads to Pentads

Monad-Diad

$$A = AA + 1/2(AB+BA)$$
$$B = BB + 1/2(AB+BA)$$

Diad-Triad

$$AA = AAA + 1/2(BAA+AAB)$$
$$(BA+AB) = BAB + 1/2(BAA+AAB) + ABA + 1/2(ABB+BBA)$$
$$= 2BAB + (BAA+AAB) = 2ABA + (ABB+BBA)$$
$$BB = BBB + 1/2(ABB+BBA)$$

Triad-Tetrad

$$AAA = AAAA + 1/2(BAAA+AAAB)$$
$$BAA+AAB = BAAB + 1/2(BAAA+AAAB) + 1/2(AABA+ABAA) + 1/2(BBAA+AABB)$$
$$= 2BAAB + (BAAA+AAAB) = (AABA+ABAA) + (BBAA+AABB)$$
$$BAB = 1/2(BABA+ABAB) + 1/2(BABB+BBAB)$$
$$ABA = 1/2(BABA+ABAB) + 1/2(ABAA+AABA)$$
$$ABB+BBA = ABBA + 1/2(ABBB+BBBA) + 1/2(BBAB+BABB) + 1/2(AABB+BBAA)$$
$$= 2ABBA + (ABBB+BBBA) = (BBAB+BABB) + (AABB+BBAA)$$
$$BBB = BBBB + 1/2(ABBB+BBBA)$$

(continued)

TABLE 1 (continued)

Tetrad-Pentad

```
      AAAA = AAAAA + 1/2(BAAAA+AAAAB)
BAAA+AAAB = BAAAB + 1/2(BAAAA+AAAAB) + 1/2(BBAAA+AAABB) + 1/2(ABAAA+AAABA)
      BAAB = 1/2(BAABA+ABAAB) + 1/2(BAABB+BBAAB)

AABA+ABAA = AABAA + 1/2(AAABA+ABAAA) + 1/2(BAABA+ABAAB) + 1/2(AABAB+BABAA)
AABB+BBAA = 1/2(AABBB+BBBAA) + 1/2(AABBA+ABBAA) + 1/2(BAABB+BBAAB) + 1/2(AAABB+BBAAA)
BABA+ABAB = BABAB + 1/2(BABAA+AABAB) + ABABA + 1/2(ABABB+BBABA)
BBAB+BABB = BBABB + 1/2(BBABA+ABABB) + 1/2(BBBAB+BABBB) + 1/2(ABBAB+BABBA)

      ABBA = 1/2(ABBAB+BABBA) + 1/2(ABBAA+AABBA)
BBBA+ABBB = ABBBA + 1/2(BBBBA+ABBBB) + 1/2(BBBAB+BABBB) + 1/2(BBBAA+AABBB)
      BBBB = BBBBB + 1/2(BBBBA+ABBBB)
```


The sequence number is given by

$$\text{Sequence number} = \Sigma A_i = \Sigma B_i = 1/2(AB+BA) \qquad (12)$$

which is

$$= 1/2(16) = 8$$

In the model chain. The average sequence lengths can be determined from Eqs. (6) and (7) with the information given by the diad distribution, that is,

$$\text{"A" average sequence length} = [2AA/(AB+BA)] + 1 \qquad (13)$$

$$\text{"B" average sequence length} = [2BB/(AB+BA)] + 1 \qquad (14)$$

Thus it can be seen that a diad distribution can be utilized to yield the same structural information as obtained from the complete sequence distribution over all possible run lengths, that is, comonomer contents, average sequence lengths, run numbers, and sequence numbers.

It is necessary at this point to make some delineating comments concerning run numbers versus sequence numbers. Generally, a diad distribution is normalized unless the degree of polymerization can be determined from the NMR data, which is sometimes the case when endgroup resonances can be identified. With normalized distributions, the composition is expressed as mole % "A" and mole % "B," and both the run number and sequence number are expressed per 100 repeat units. For copolymers where the "B" repeat unit is substantially lower in concentration than the "A" repeat units, the mole percent "B" will be the same as the sequence number if all of the "B" units are isolated. In other words, the extent of "clustering" of "B" units as BB, BBB, etc. can be determined directly by comparing the sequence number to the total mole percent "B." Another important point is that the "run number" is always used mathematically, when reducing n-ad distributions to useful structural information, as 1/2 the run number. It is normally the number of sequences of each type and not necessarily the total that is the more important information. This point is emphasized in

analyses involving triad and higher order *n*-ad distributions because the sequence number can be determined independently from A-centered and B-centered *n*-ad distributions. This result is an important verification of the reliability of the NMR data experimentally as will be seen later in discussions of analyses of linear low-density polyethylenes. Although it may at first appear pedantic, a review will be given of the triad distribution to demonstrate this very point.

A triad distribution is easier to develop conceptually because each repeat unit is the center unit of a unique triad. The A-centered and B-centered triads are identified below for the same model chain used in the previous arithmetic developments utilizing, initially, the complete sequence distribution and, secondly, the diad distribution.

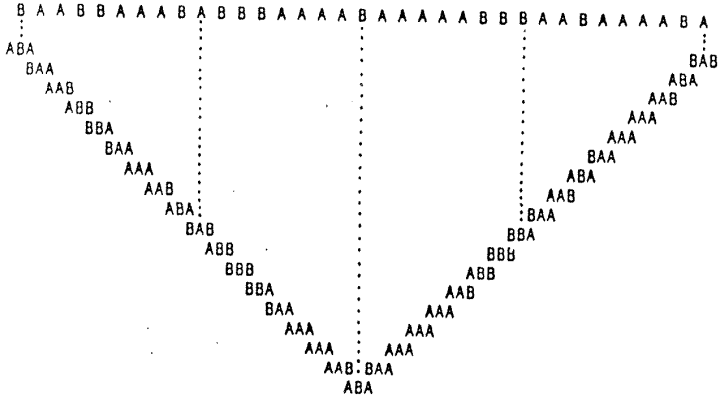

The triads total as follows:

AAA = 8	BBB = 2
AAB+BAA = 12	ABB+BBA = 6
BAB = 2	ABA = 5

The triads are grouped by like centers because the complete sets of A-centered triads and B-centered triads represent, respectively, all of the possible arrangements for the neighboring units of the "A" and "B" repeat units. Consequently, the total number of "A" units and the total number of "B" units are given by

$$A = \Sigma A_i = AAA + (BAA+AAB) + BAB = 22 \quad (15)$$

and

$$B = \Sigma B_i = BBB + (ABB+BBA) + ABA = 13 \quad (16)$$

The sequence numbers are likewise given by

$$\Sigma A_i = BAB + 1/2(BAA+AAB) \quad (17)$$

$$\Sigma B_i = ABA + 1/2(ABB+BBA) \quad (18)$$

Equation (17) is easy to visualize conceptually because BAB gives the concentration for the sequence length of one while 1/2(BAA+AAB) gives the collective concentration of all of the remaining sequences because each sequence of two and longer begins with BAA and ends with AAB. The analogous situation produces Eq. (18). As was the case for the diad distribution, it was possible to determine the total number of sequences per chain or for any specified number of repeat units without knowing the length of the longest sequence in the chain. The triad distribution is more valuable experimentally than a diad distribution because the sequence number can be determined independently from the A-centered and B-centered triads as shown above by Eqs. (17) and (18). In later discussions involving experimental triad distributions from ^{13}C-NMR data of various copolymers, this relationship will be used to check the reliability of the NMR data.

The average sequence lengths, in terms of triads, are given by

$$\text{"A" average sequence length} = [AAA + (BAA+AAB) + BAB]/[BAB + 1/2(BAA+AAB)] = 22/8 = 2.75 \quad (19)$$

and

$$\text{"B" average sequence length} = [BBB + (ABB+BBA) + ABA]/[ABA + 1/2(ABB+BBA)] = 13/8 = 1.625 \quad (20)$$

Several new "necessary relationships" are derived from the equations for the diad and triad distributions. For example, Eqs. (12), (17) and (12), (18) give, respectively,

$$(AB+BA) = 2BAB + (BAA+AAB) \quad (21)$$

$$(AB+BA) = 2ABA + (ABB+BBA) \quad (22)$$

and

$$2BAB + (BAA+AAB) = 2ABA + (ABB+BBA) \quad (23)$$

or

$$(AB+BA) = BAB + 1/2(BAA+AAB) + ABA + 1/2(ABB+BBA) \quad (24)$$

From Eqs. (9), (15), (21) and (10), (16), (22), respectively, the following additional relationships are obtained:

$$AA = AAA + 1/2(BAA+AAB) \quad (25)$$

$$BB = BBB + 1/2(ABB+BBA) \quad (26)$$

The necessary relationships between higher order n-ads can be derived in exactly the same manner as just demonstrated for diads and triads. Table 1 contains all of the necessary relationships from monads to pentads. These necessary relationships can be obtained by inspection through the realization that each $(n + 1)$-ad contains two n-ad sequences.

In each of the previous examples, the actual numbers of n-ads per chain were utilized to obtain average sequence lengths, total numbers of "A" and "B" repeat units per chain, sequence numbers per chain, and run numbers. In practice, the concentrations used in handling necessary relationships are mole fractions or, more preferably, n-ad fractions. Normalization is required of NMR data unless, as stated previously, endgroup resonances can be identified and measured quantitatively. Thus normalized sets of n-ad fractions are typically obtained following a sequence analyses based on NMR data.

What is sometimes overlooked in ^{13}C-NMR analyses of sequence distributions is the usefulness of the total n-ad intensity, which is used to normalize the n-ad data. Because of the necessary relationships, any complete n-ad distribution will sum to the same total n-ad intensity. Thus once a particular total n-ad intensity is obtained, it can be used to normalize any partial n-ad data set. This is an important result because complete tetrad, pentad, or higher order n-ad distributions are seldom obtained. The partial sets can be utilized in statistical analyses to check the adequacy of a particular statistical model or "fit." If endgroup intensity data are available, the number of sequences per chain can be directly determined as well as the degree of polymerization or number-average molecular weight [5].

It is now obvious that what is needed to perform a polymer sequence distributional analysis is any n-ad set higher than monads. Too often the NMR analyst tries to obtain as many n-ad sets as possible and at the highest possible order, sometimes sacrificing accuracy to do so. A copolymer sequence distributional analysis over any particular set of n-ads greater than one will yield the relative concentrations of "A" and "B," average sequence lengths for "A" and "B," the run number, the sequence number, and, in special cases, the degree of polymerization. Unfortunately, ^{13}C NMR does not possess the required sensitivity to lend to a distributional analysis over all

Case 1:05-cv-00737-JJF Document 160-5 Filed 09/03/2008 Page 26 of 42

EXHIBIT PAGE 001001

possible sequence lengths, as shown in the first model analysis. What is more important is to obtain an accurate result, which can be done if the most reliable *n*-ad distribution available is selected for analysis. The necessary relationships are an indispensable ingredient for reducing NMR information, responsive to sequence lengths from two to as many as seven or nine contiguous units, to a complete set over a specific *n*-ad length.

In the ensuing discussions, sequence analyses of the following specific ethylene-based polymers will be given: ethylene/propylene copolymers; the three most important commercial linear low-density polyethylenes (ethylene–1-butene, ethylene–1-hexene, and ethylene–1-octene copolymers); high-pressure, low-density polyethylenes; and ethylene/vinyl acetate copolymers, which are also produced in a high-pressure process. Long-chain branching will be discussed not only in the polymers produced in the high-pressure processes but also as an unplanned structural moieties in high-density, linear polyethylenes. Discussions of experimental NMR conditions, assignments, and equipment will be introduced in the following section. At this point, it is important to emphasize how information is obtained and then proceed to data manipulations later without placing too great an emphasis on ^{13}C NMR from a phenomenological viewpoint. Any other required prerequisites will be introduced simply and briefly as needed throughout the discussions.

II. EXPERIMENTAL

Phenomenological descriptions of both conventional continuous wave and Fourier transform nuclear magnetic resonance techniques have been well described previously [8, 10] and will not be repeated in this article. There are, however, some prerequisites for practical considerations worthy of further discussion when investigating macromolecules. These are NMR acquisition conditions, experimental efficiency, dynamic range, and optimized sample solution concentrations and temperatures with respect to experimental running conditions. Carbon-13 NMR data are efficiently collected in the time domain and then mathematically separated into its frequency domain through Fourier transformation after data acquisition is complete. The choices for data acquisition conditions are critical if an efficient and quantitatively reliable experiment is to be performed.

In a typical NMR experiment, in the time domain the sample is excited by a long series of strong, square-wave radiofrequency pulses of very short duration. If properly

chosen with respect to both frequency and duration, each pulse will "tip" the local nuclear moments by a predetermined angle, usually 90°, after which the local moments will return to their previous state prior to excitation by a process described as free induction decay (FID). The spacings between the rf pulses should be such that the assembly of nuclear spins can return to equilibrium before the next pulse is applied. Free induction decay can be observed by placing a received coil in a direction orthogonal to the applied rf pulse. If the rf pulse frequency and nuclear spin precessional frequency perfectly coincide, resonance is achieved and a pure exponential will be observed for the FID [8]. Normally, a more complex FID pattern analogous to "ringing" in the continuous wave experiment is observed because the applied rf pulse is necessarily off-resonance for most organic moieties, which typically exhibit spectral lines within a 200 ppm range from an internal tetramethylsilane (TMS) standard. Time constants for FID are determined along two axes in the rotating frame [8], the field axis or "z" direction and the orthogonal xy plane. The former is called longitudinal relaxation, and the time constant for decay is the spin-lattice relaxation time, T_1. Decay in the orthogonal direction is known as transverse relaxation, and the decay constant is called the spin-spin relaxation time, T_2.

As the names for these decay constants imply, different mechanisms are responsible for nuclear relaxation in the transverse and longitudinal directions. Spin-lattice relaxation depends upon the strength of coupling between the nuclear spin system and the "lattice" to which it belongs, and is governed by local, fluctuating magnetic fields with components orthogonal to the main field direction. Spin-spin relaxation times may contain a contribution from field inhomogeneity and depend upon local molecular motions with components in all three directions. In general, low-frequency processes or molecular motions will only affect T_2 while high-frequency processes will affect both T_1 and T_2. The appropriate time spacing between pulses in a long train of pulses during NMR data acquisition depends upon T_1 [8]. For polymers, T_1 will typically vary between 10^{-1} and 10^{2} s. To ensure 99% relaxation, the pulse spacing should be $5 \times T_1$ for the longest observed T_1 [8]. For some polymer systems this could lead to an inordinate amount of time for data accumulation, and there are times when a decision must be made as to whether the information acquired should only be used for qualitative purposes.

Quantitative measurements require either complete relaxation or identical amounts of partial relaxation to obtain reliable results. In the development of quantitative procedures, it is usually prudent to select those resonances for analysis where relaxation requirements have been stringently met.

Considerable polymer spin-lattice relaxation time data are available in the literature. A typical range of molecular mobilities is represented by polyethylene [11], polypropylene [12, 13], and polystyrene [9, 14]. The observed T_1's can be conveniently and directly related to the extent local, fluctuating segmental motions contribute to the relaxation process. For example, slower rates of relaxation or longer "time constants" are observed for carbons close to the ends of short side-chain branches or at the ends of the polymer chain. Shorter T_1's are observed for interior carbons in long, recurring methylene sequences or adjacent to a branch [11]. In ethylene–1-hexene copolymers, for example, the recurring methylene carbons from long, uninterrupted ethylene sequences exhibit a T_1 of 1.9 s at 118°C [11]. The carbons at the ends of butyl branches exhibit a T_1 of 4.4 s while the carbons next to the branches uniformly exhibit T_1's of approximately 1 s [11]. In low-density polyethylenes, prepared in high-pressure processes, the overall chain structure has created considerably more local segmental motions than found in the higher density ethylene–1-hexene copolymer described above. The methyl carbons from the butyl branch in this case display a T_1 of 7.1 s [11]. Very short T_1's are observed for polymers with considerable side-chain steric hindrance. Both the backbone and side-chain carbons in polystyrene exhibit extremely short T_1's of approximately 0.1 to 0.2 s at 40–44°C [9, 14]. The longest observed T_1 in polystyrene occurs for the ring quaternary carbons, which have no directly bonded protons to contribute to the relaxation process [9]. Fortunately, there is enough information presently in the literature to make some well-educated guesses as to the proper pulse spacing in the long train of pulses required to generate ^{13}C-NMR polymer spectra from the Fourier transform type of NMR experiment.

Although of equal importance, there has been up to now less attention paid to the measurement of spin-spin relaxation times or T_2's in NMR solution studies of polymers. Line widths of ^{13}C-NMR polymer spectra vary strongly with both concentration and temperature [15]. Also, line widths are not necessarily uniform so the use of peak heights in quantitative measurements can yield misleading results. A comparison of peak height to peak area measurements is given in Table 2 for the endgroup resonances from NBS 1475 polyethylene, which is known to have a number-average molecular weight around 18,000. At temperatures close to 125°C and at concentrations under 15% by weight, line widths of less than 1 Hertz at one-half the peak height can be obtained with an optimized magnetic field. In molten polymers or swollen gels where the polymer concentrations approach 50% or better by weight, line widths at one-half height may exceed 10 Hertz.

Most investigators assume that the sample conditions in the typical NMR experiment used for polymers lead to a condition known as "extreme narrowing" [16, 17], where T_1 is the same as T_2 and independent of the applied frequency. Under extreme narrowing, NOE's should also be full [13, 16, 18]. As a consequence of an exclusive dipole-dipole relaxation mechanism [14, 19], T_1 should increase with increasing temperature [8].

TABLE 2

A Comparison of Resonance Intensities as Measured by Peak Heights and Peak Areas for NBS 1475 Polyethylene

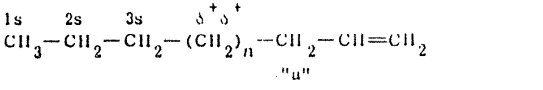

Carbon	Peak height (mm)	Normalized peak area
1s	40.5	0.91
2s	50.7	0.88
3s	56.9	1.04
$\delta^+\delta^+$	30,000	902.4
"a"	19.4	0.48
M_n (calculated)	12,300	17,800
M_n (observed)	18,300	18,300

There is considerable evidence in the literature to suggest that these conditions are met in dilute solutions and at temperatures in a range of 100–150°C. It has been reported that even molten polyethylene exhibits a full NOE, which suggests a condition of "extreme narrowing" [17]. Nuclear Overhauser effects occur only during proton-carbon heteronuclear spin decoupling, which removes all proton spin coupling interactions with ^{13}C nuclei during data acquisition. Under such circumstances, energy transfer can occur from the proton to the carbon nuclear spin system and create enhanced ^{13}C resonance intensities by a factor of 3 for full NOE's. The NOE represents a bonus when ^{13}C-NMR experiments are performed to detect structural moieties in a range of one to ten per 10,000 carbon atoms. Full NOE's are typically observed in polymer ^{13}C-NMR spectra as a consequence of a relaxation process totally dominated by the dipole-dipole mechanism [19].

Another consideration equally important to molecular dynamics for a properly designed FT-NMR experiment for polymers is dynamic range. During a train of rf pulses, each FID is recorded and stored arithmetically at a preset computer memory location. Signal-to-noise averaging occurs because the weak ^{13}C-NMR signals continue to give a positive response while the noise signals add in a random manner. The final signal-to-noise improvement is equal to the square root of the number of accumulated FID's. At the outset of data accumulation, the spectrometer gain setting should be such that the FID just fills the receiver. The strongest time domain signal should not be clipped. The receiver analog-to-digital conversion, ADC, should be in a range of 13–15 bits including sign. Each additional ADC bit doubles the size of the FID that can be digitized; however, this requirement is not so stringent as the wordsize in memory where the FID's are stored arithmetically. For example, if one has only a 16-bit word and wishes to average FID's where the signals in the time domain have a 1000 to 1 peak height ratio, 10 bits of that word are required to record the first FID if the weakest signal requires only one bit of storage. After the additional accumulation of only 31 FID's, the computer word is completely filled and from that point on the data in memory will be truncated to accommodate further storage of FID's. Most systems shift one bit, which is equivalent to dividing the data by a factor of 2, after the wordsize is filled. Even if the receiver capability were 10^5 to 1, the data could not be recorded with sufficient precision to ensure a

correct observation. This problem is easily solved by using double precision arithmetic during data acquisition. Under such circumstances, 2^{21} FID's can be recorded in a 1000/1 experiment before the wordsize is exhausted. The need to satisfy dynamic range requirements for at least a 1000 to 1 signal ratio occurs frequently in FT-NMR studies of polymers. Typical commercial polyethylenes, for example, have number-average molecular weights between 10,000 and 20,000, corresponding to molecular carbon numbers between 700 and 1500. If end carbon resonances or branching in a range of one per polymer molecule are to be reliably observed, the FT-NMR experiment must meet the proper dynamic range requirements. Finally, the effect of choice of solvent on dynamic range requirements should not be overlooked. Frequently the solvent used in polymer ^{13}C-NMR experiments gives rise to strong ^{13}C-NMR signals of its own. It is possible for the memory available for time averaging to become extremely limited if floating point arithmetic cannot be used during data averaging.

It has also been recognized that the attainment of ^{13}C-NMR spectra with high dynamic range requirements also requires an appropriate handling of the Fourier transform calculation. Round-off errors can seriously distort spectra when peak intensity ratios are 1000 to 1 or higher. This problem has been diverted by using floating point arithmetic during Fourier transform calculations [20]. With considerable attention paid to both instrumental and mathematical distortions possible in FT-NMR experiments, excellent results can be attained in quantitative studies of polymers. The future looks even brighter with well-designed probes [21] and faster, more efficient and larger, yet cost effective computer systems.

A final, and perhaps the most important, consideration in planning high-quality polymer ^{13}C-NMR experiments is sample preparation. High-quality spectra with narrow line widths necessary for quantitative measurements can be easily and routinely obtained. In the interest of efficiency, polymers are sometimes examined in FT NMR experiments as swollen gels or in the molten state. The resulting spectra exhibit very broad line widths, sometimes exceeding 10 Hz at the one-half peak height for 50 MHz spectra obtained at 125°C, when the solution concentrations are 50% or greater weight percent polymer. An example of how the apparent resolution can be considerably reduced by concentration for a polyethylene is shown in Table 3. Second, if the polymer spectrum is dominated by a single,

TABLE 3

Line Widths at One-Half the Peak Height for the Major Resonances of Marlex PE 6003 as a Function of Concentration (50 MHz data at 124°C)

Resonance	15% by weight polymer solution	50% by weight polymer solution
1s	0.6 Hz	5.6 Hz
2s	0.6	3.8
3s	0.6	—
α	0.6	6.3*
$\delta^+\delta^+$	0.8	10.1

*Affected by the tail of the major $\delta^+\delta^+$ resonance and could not be accurately determined.

strong resonance as in the case of polyethylene, the Lorentzian character of the main resonance leads to strong "tails" extending as far as 3–5 ppm from the center of the major resonance. When this happens, it is difficult to obtain true intensity measurements free of contributions from this "tree-trunk" effect. At solution concentrations of less than 15 wt% polymer, the lines can become exceedingly narrow and an optimum resolution is achieved as illustrated in Table 3. The observed lines will broaden, and selectively so, as the polymer weight percent in solution is increased. The use of peak heights for quantitative measurements can become totally unreliable for solutions containing 20 or more weight percent polymer. An example of such an effect is shown in Fig. 1 for the same polymer at 15 and 50 wt% in 1,2,4-trichlorobenzene at 125°C. The change to broader line widths at higher concentrations suggests that the condition of "extreme narrowing" may only exist in dilute solutions. At higher polymer concentrations where there is restricted mobility, T_2 may be less than T_1. Certainly more dynamic ^{13}C-NMR measurements on polymers are needed as a function of concentration and temperature as well as applied field before the observed line-width behavior is fully understood.

Finally, the choice of solvents may slightly influence polymer ^{13}C-NMR chemical shifts. This point is illustrated by

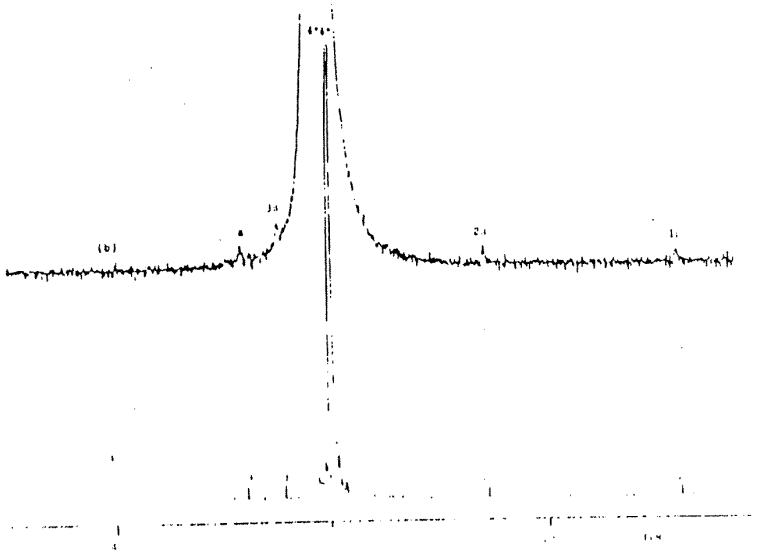

FIG. 1. Marlex 6003 at (a) 15% by weight and (b) 50% by weight in 1,2,4-trichlorobenzene at 125°C.

tabulating the chemical shift data from many of the various ethylene-based copolymers and homopolymers in two solvents, trichlorobenzene/benzene-d_6 and tetrachloroethane-d_2. In each case the observed chemical shifts are corrected to an internal tetramethylsilane standard by setting the major, recurring methylene resonance to 29.98 ppm.

III. NOMENCLATURE

In the introductory section, copolymeric units were designated simply by "A" and "B" and the various possible A,B sequence arrangements identified. In the following sections, quantitative NMR analyses of ethylene–propylene,

Case 1:05-cv-00737-JJF Document 160-5 Filed 09/03/2008 Page 30 of 42

EXHIBIT PAGE 001005

ethylene–1-butene, ethylene–1-hexene, and ethylene–1-octene copolymers will be discussed in detail. The nomenclature employed will be "E" for ethylene, "P" for propylene, "H" for 1-hexene, and "O" for 1-octene in descriptions of sequence distributions. A more specific nomenclature is required as opposed to the general A,B nomenclature to both differentiate and compare homologous sequences among the various copolymers.

In contrast to step-growth polymers where functional groups or hetero atoms allow the individual repeat units to be identified, the monomer identity is "lost" in chain-growth polymers such as a poly(1-olefin) or an ethylene–1-olefin copolymer. For example, a "poly(ethylene)" is actually a long chain of methylene sequences, and, in "poly(propylene)," head-to-tail versus tail-to-head repeat unit sequences cannot be distinguished when there are no repeat unit inversions. In ethylene–1-olefin copolymers where 1-olefin inversion can occur, the sequence descriptions may not be unique. For example, in ethylene–propylene copolymers, a $\bar{P}$ P sequence cannot be distinguished from a P E $\bar{P}$ sequence [22–25], that is,

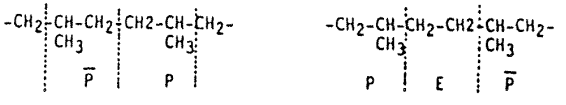

Since the above molecular structures are the same and it is only the sequence descriptions that differ, it must be pointed out that ^{13}C-NMR resonances from polymers arise from carbon atoms in specific structural environments, and it is up to the polymer chemist to translate a carbon resonance identification to an identification of the precise sequence in which it resides. A carbon atom nomenclature is needed, therefore, in addition to a sequence identification. Out of necessity, a nomenclature system initiated by Randall [26] and nicely expanded by Carman [22] has slowly evolved over the years. Methylene carbons located along the backbone of an ethylene–1-olefin copolymer chain are identified by a pair of Greek letters, indicating the locations of the nearest methine carbons in either direction. The Greek letter α indicates that a methine carbon is bonded to a methylene carbon of interest. Two Greek letters, αα, indicate that the identified methylene carbon is sandwiched between two methine carbons. A β indicates that a methine carbon is two carbons removed from the carbon of

interest, and so forth. Since neighboring carbon contributions to chemical shifts seldom exceed four carbons removed, a methine carbon four or more carbons from the methylene carbon of interest is indicated by a δ^+. The following structural sequences give characteristic methylene resonances in ^{13}C-NMR spectra of ethylene–1-olefin copolymers:

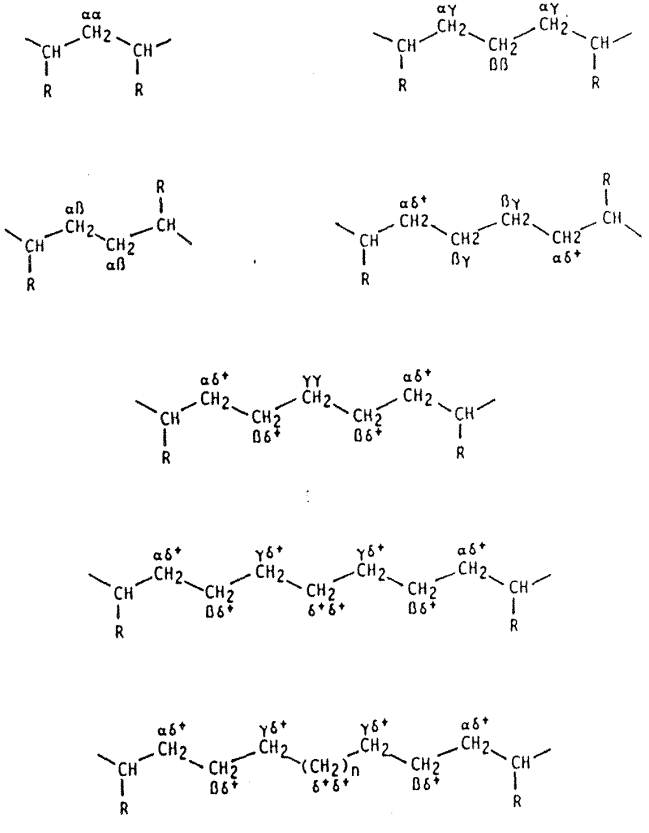

Methine and side-chain carbons from short-chain branches are identified as the center unit of either a triad, pentad, etc. sequence, whichever is appropriate. (Note that methine and side-chain carbons will be sensitive to odd membered *n*-ad sequences only.) As a further illustration, the three types of methine carbons are identified for an ethylene–propylene copolymer below:

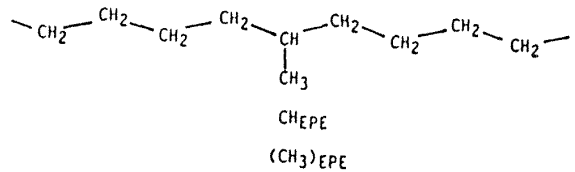

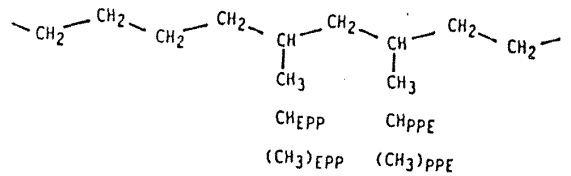

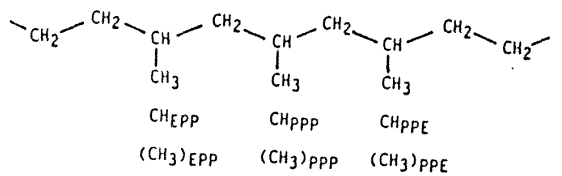

The methine carbons and methyl branches, above, are identified according to the sequence in which they are located. It is also necessary to identify the location of each carbon in the various types of branches. Carbons in side-chain branches are identified by iB_n where "*i*" designates the position in the branch starting with the methyl carbon as "1." The subscript "*n*" is used to designate the length of the branch, as illustrated here:

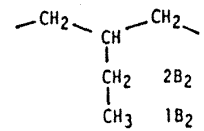

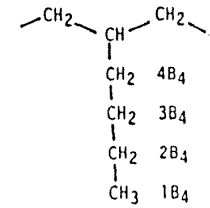

Examples of where both the sequence and branch carbon are identified would be $(1B_2)_{EBE}$, $(1B_2)_{EBB+BBE}$, and $(1B_2)_{BBB}$, as can be found in an ethylene–1-butene copolymer containing both isolated and blocked 1-butene sequences.

Polyethylene endgroup resonances may be typically observed after only a few hours running time thanks to the newer generations of Fourier transform NMR spectrometers. As stated previously, a detection of structural entities at levels of 1/1000 and 1/10,000 and lower are possible. As shown in Table 2, the saturated endgroup carbons in polyethylene are designated as 1s, 2s, and 3s starting with the methyl end group carbon as "1." The carbon allylic to a terminal vinyl group is designated as "a."

IV. ASSIGNMENTS

Assignments are the key to a successful copolymer quantitative analysis, but there is not always agreement among various workers as to which assignments are correct. Model copolymers offer the best approach but are not always available. Off-resonance decoupling can be used to distinguish carbons by the number of directly bonded protons, but it does not always lead to unequivocal choices. The methods of choice for identifying carbon types in ^{13}C-NMR spectra are the various sophisticated pulse sequences, which can be used in complex polymer systems with far less ambiguity than encountered with off-resonance decoupling. APT [27] and INEPT [28, 29], which stand for "Attached Proton Test" and "Insensitive Nuclei Enhancement by Polarization Transfer," respectively, involve the use of amplitude modulations introduced into noise-decoupled

^{13}C-NMR spectra by heteronuclear J couplings. In the APT test, methyl and methine carbon resonances will have an opposite sign to methylene and quaternary carbon resonances. The identification is unambiguous. When proton-coupled ^{13}C-NMR spectra are investigated by the INEPT method, the usual intensity ratios for multiplets no longer apply. The methine carbons respond with a −1:1 intensity ratio, methylene carbons give a −1:0:1 ratio, and methyl carbons give a −1:−1:1:1 ratio [30].

The generation of ^{13}C-NMR subspectra, which are sorted by carbon resonance multiplicity, has been best optimized through the development of the DEPT (Distortionless Enhancement by Polarization Transfer) technique [31, 32]. It may be beneficial to discuss the DEPT technique in somewhat more detail than APT and INEPT because it is becoming accepted as the state-of-the-art technique. "DEPT" also has the additional and valuable benefit of yielding sensitivity enhanced ^{13}C-NMR spectra. The basic DEPT pulse sequence is given below [31]:

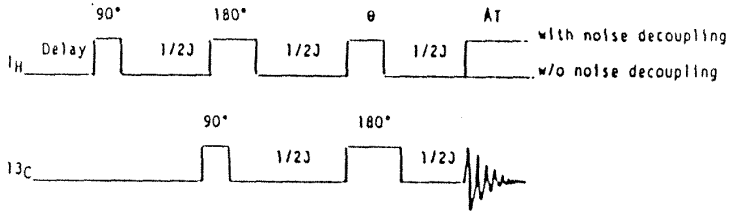

The DEPT technique also utilizes phase modulation introduced by ^{13}C-^{1}H scalar coupling and refocusing pulses similar to the APT and INEPT methods. After an appropriate delay to ensure the proton spin states have reached equilibrium, the ^{1}H spins are pulsed 90°. A delay of $1/(2J)$ is introduced (where J is the correct ^{13}C-^{1}H scalar coupling constant) to permit phase modulation. The ^{1}H spins are then refocused with a 180° pulse while the ^{13}C spins are pulsed 90° for the first time. A second delay of $1/(2J)$ is introduced for both spin systems, after which the ^{13}C spins are refocused with a 180° pulse while the ^{1}H system is simultaneously pulsed at an

angle θ. If the θ pulse is phase shifted with respect to the first 90° pulse, transfer of polarization is achieved from the ^{1}H to the ^{13}C spins. A maximum enhancement occurs for the methine carbons at θ = 90°, the methylene carbons at 45°, and the methyl carbons at 35°. An advantage of the DEPT technique over APT and INEPT is that both the coupled and ^{1}H-noise decoupled spectra have a normal appearance with no differences in enhancement factors for different lines within a multiplet in coupled spectra as observed with APT and INEPT. A significant feature of DEPT is that specific carbon multiplicities can be observed while suppressing other types, that is, CH_3 versus CH_2 versus CH through addition of spectra taken at appropriate θ angles. This technique is referred to as "DEPT spectrum editing" or "ADEPT." The latest generations of NMR spectrometers have the advanced ADEPT technique that automatically sorts spectra by carbon resonance multiplicity and presents separate printouts for methyl, methylene, and methine carbons. This discussion represents only a brief review of the state-of-the-art of carbon type determinations, but it does demonstrate that any one of several possible pulse sequencing techniques can lead to an unequivocal sorting of carbon resonance multiplicities. An example of spectral editing is given in Fig. 2 for a low-density polyethylene produced in a high pressure reactor.

The next step in establishing ^{13}C NMR polymer assignments is to review briefly the available methods for distinguishing among carbon atoms having the same number of directly bonded protons. The Grant and Paul parameters [33] historically are of great importance because it was the pioneering method for chemical shift assignments in ^{13}C-NMR spectra of both organic compounds and macromolecules. A number of modifications and improvements were later introduced [34–36]; however, it was Tonelli [37] who demonstrated that the number of empirical parameters required by Grant and Paul and others [36] were simply a manifestation of differences among nonbonded local interactions. A consideration of rotational states and the number of three-bond γ interactions elegantly account for many of the chemical shift differences observed in ^{13}C-NMR spectra of macromolecules [37, 38]. Tonelli used the Suter-Flory [39] model of polypropylene, which is a five-state model where each backbone bond is permitted to adopt any of the t, t^*, g^*, g, or $\bar{g}$ states corresponding to bond rotation angles of 15, 50, 70, 105, and 115°, respectively, to calculate the configurational chemical shift differences for each carbon in polypropylene and a series of

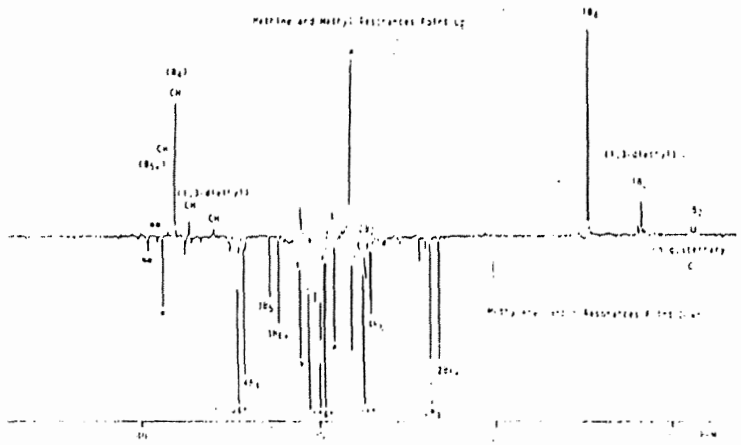

FIG. 2. A "DEPT" carbon-13 NMR spectrum of an LDPE at 50.3 MHz at 125°C in tetrachloroethane-d_2.

model compounds [40–42]. A single γ parameter of −5.3 ppm successfully accounted for the observed experimental chemical shift differences. The Grant and Paul parameters have built in the γ interactions through the number of direct parameters (α through ε) and the subsequent "corrective terms." If one realizes that the Grant and Paul approach is strictly empirical and an oversimplification, it can still be usefully applied in NMR studies of macromolecules. The Tonelli method does require computer facilities to generate the required information for assignment purposes while the Grant and Paul method can be performed with a pocket calculator. A brief overview of the Grant and Paul method, therefore, would be useful.

Carbon-13 NMR chemical shifts can be calculated based on the proximity and number of near neighboring carbon atoms in terms of parameters derived from the chemical shift behavior observed for an extensive set of both linear and branched alkanes [33]. The reference point is methane and corrections are made to the methane chemical shift according to the number and geometry of neighboring carbon atoms. The contribution

of directly bonded carbon atoms to the methane chemical shift is "α," the contribution from carbons two bonds removed is "β," the contribution from carbons three bonds removed is "γ," the contribution from carbons four bonds removed is "δ," and, finally, the contribution from carbons five bonds removed is "ε." "Corrective terms" are also included to account for steric or geometrical differences. In the corrective terms, quaternary, tertiary, secondary, and primary carbons are designated as 4°, 3°, 2°, and 1°, respectively. Descriptively, the carbon of interest is placed first in the corrective term and the contributing carbon is listed second in parentheses. The calculated chemical shift for the methine carbon in the example below is:

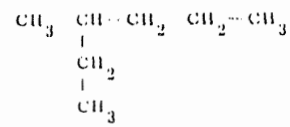

$$\text{methine chemical shift} = CH_4 + 3\alpha + 2\beta + \gamma + 2[3^\circ(2^\circ)] + 3^\circ(1^\circ) \qquad (27)$$

The basic Grant and Paul parameters and some of the more useful corrective terms are given in Table 4. Some alternative additive schemes [36] and some improvements [34, 35] have been given in the literature; however, there is a limit to which these or any other parameter systems can be usefully applied. The original Grant and Paul parameters will delineate basic structural differences but cannot be used for differentiating subtle chemical shift differences of 1.0 ppm or less.

A proper application of the Grant and Paul parameters can best be illustrated by using the parameters in Table 4 to calculate the chemical shifts for the ethylene–propylene copolymer sequences listed later in Table 6. (The assignments in ethylene–propylene copolymers will be discussed in detail in the following section.) Calculated versus experimental results are given in Table 5. The calculated chemical shifts for the different types of methylene carbons are in the correct order from low to high field, that is,

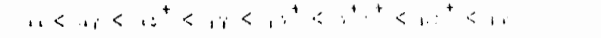

TABLE 4

The Grant and Paul Parameters for Alkanes Which Are Most Often Applied in Analyses of ^{13}C-NMR Spectra of Macromolecules

α =	9.09 ppm	$3°(2°)$ =	−3.65 ppm
β =	9.40	$2°(3°)$ =	−2.50
γ =	−2.49	$1°(3°)$ =	−1.12
δ =	0.31	$3°(1°)$ =	0.00
ϵ =	0.11	CH_4 =	2.97[a]

[a] With respect to TMS.

The methine carbon chemical shifts are in the right order but out of place with respect to the remaining chemical shifts:

$$CH_{EPE} < CH_{EPP+PPE} < CH_{PPP}$$

The calculated chemical shifts for the four methyl carbon sequences fall correctly in the observed order:

$$(CH_3)_{PPPPP} < (CH_3)_{EPPPP+PPPPE} < (CH_3)_{PPPEP+PEPPP} < (CH_3)_{EPE}$$

What is not correct for the calculated versus observed methylene carbon chemical shifts is the delineations between the two types of $\alpha\delta^+$ sequences, the two types of $\beta\delta^+$ sequences, and the three types of $\beta\beta$ sequences. While the methine chemical shifts are not only incorrectly predicted as to where they should appear relative to the remaining methylene chemical shifts, the calculated values differ by more than a ppm from the observed values. The reasons for these differences probably arise first from the possibility that the "corrective terms" for alkanes cannot be indiscriminately applied to polymers [33] and

TABLE 5

Carbon-13 NMR Chemical Shifts with Respect to an Internal Tetramethylsilane Standard Calculated with the Grant and Paul Parameters for the Ethylene–Propylene Copolymer Sequences Listed in Table 6

Observed chemical shifts	Calculated chemical shifts	Carbon assignments	Sequence assignments
46.52	44.29	$\alpha\alpha$	PPPP (mmm)
46.06	43.98	$\alpha\alpha$	PPPE+EPPP (mm)
45.77	43.67	$\alpha\alpha$	EPPE (m)
37.91	37.39	$\alpha\gamma$	PPEP+PEPP (mm)
37.89	37.08	$\alpha\gamma$	EPEP+PEPE (m)
37.51	36.77	$\alpha\delta^+$	EPEE+EEPE
37.46	37.08	$\alpha\delta^+$	PPEE+EEPP (m)
33.22	31.66	Methine	EPE
30.95	29.17	Methine	EPP+PPE
30.77	30.49	$\gamma\gamma$	PEEP
30.36	30.18	$\gamma\delta^+$	PEEE+EEEP
29.98	29.87	$\delta^+\delta^+$	$(EEE)_n$
28.91	26.68	Methine	PPP (mm)
27.43	27.38	$\beta\delta^+$	EPEE+EEPE
27.28	27.49	$\beta\delta^+$	PPEE+EEPP (m)
24.85	24.89	$\beta\beta$	EPEPE (m)
24.71	25.00	$\beta\beta$	EPEPP+PPEPE (mm)
24.56	25.11	$\beta\beta$	PPEPP (mmm)
21.83	20.50	Methyl	PPPPP (mmmm)
21.61	20.39	Methyl	PPPPE+EPPPP (mmm)
20.92	20.19	Methyl	PPPEP+PEPPP (mmm)
19.97	19.66	Methyl	EPE

second, from the likelihood that the Grant und Paul ξ und ε terms arise from differences in the "γ" conformational contributions as pointed out by Tonelli and are, therefore, not "carbon contributions." This last point is reinforced by the observed ^{13}C-NMR spectrum of the ethylene–propylene copolymer in Fig. 1 where four different $\alpha\gamma$ PPEP resonances are observed as a consequence of differences in chirality. In addition, the $\alpha\delta^+$ und $\delta\delta^+$ PPEE chemical shifts are both upfield from $\alpha\beta^+$ und $\beta\beta^+$ EPEE, which is in the opposite direction from the predicted location. The Grant und Paul "γ" und "ε" contributions lead to a prediction of downfield shifts for the more branched sequences. Nevertheless, when combined with carbon resonance multiplicity determinations und reference polymer systems, the Grant und Paul parameters can be a useful tool for making polymer ^{13}C-NMR chemical shift assignments. A general rule of thumb is that the Grant und Paul parameters can be used for tentative assignments in those cases where differences do not depend only on a "ξ" or "ε" contribution. Methine und methyl chemical shifts should always be assigned through multiplicity determinations because this is another area where the Grant und Paul "corrective terms" may not be applicable.

A discussion of assignment methods would not be complete without mentioning model compounds, which have also been useful in analysis of polymer spectra [43–45]. A model compound for a polymer should be a reasonably large molecule [41] or it will possess the same deficiencies as the Grant und Paul parameters for alkanes when applied to macromolecules. One should be very cautious about conformational contributions und be aware that sequence shifts in ^{13}C-NMR copolymer spectra can display a wide range of sensitivities routinely from diads to pentads und sometimes hexads und longer. Oligomers und polymers with rigorously controlled structures offer the best model systems when establishing chemical shift assignments und behavior [46–49].

A final area that has done a great deal to clarify NMR chemical shift assignments in both ^{1}H- und ^{13}C-NMR polymer spectra is two-dimensional NMR spectroscopy. An elucidation of overlap und multiplet structure leading to chemical shift assignments und homonuclear coupling constants in ^{1}H-NMR polymer spectra has been accomplished through two-dimensional J-resolved NMR spectroscopy [50]. Contour plots of J (Hz) versus chemical shifts in ppm lead to resolution of overlapping multiplets differing by only a few Hz. Although specific

assignments still require model compounds or reference polymers, the ability to resolve und identify the number of overlapping multiplets has given new life to ^{1}H NMR of polymers [51]. Carbon-13 NMR assignments can be made from known ^{1}H-NMR assignments through contour plots of two-dimensional ^{13}C-^{1}H correlated spectra. An excellent example of this use of two-dimensional NMR spectroscopy for assignments of monomer sequences in ethylene containing co- und terpolymers has been published by Bruch und Payne [52]. The proton assignments were confirmed by two-dimensional J-resolved NMR spectroscopy und homonuclear two-dimensional correlated spectroscopy (COSY) [52]. One of the most interesting uses of two-dimensional NMR has been in two-dimensional NOE studies of copolymer conformations [53, 54]. Although two-dimensional NMR plots sometimes take on a formidable appearance, they can often be quite reasonably und easily interpreted. This technique has become an indispensable requirement for confirming both ^{1}H- und ^{13}C-NMR sequence assignments.

V. ETHYLENE-PROPYLENE COPOLYMERS

The first in the homologous series of ethylene–1-olefin copolymers is the ethylene–propylene copolymer, of interest commercially as a rubber, a "random copolymer, und a so-called block copolymer. An ethylene–propylene rubber, known as EPR, is a random copolymer containing inverted propylene sequences und is better treated structurally as though it were a terpolymer [21]. The "random" copolymer falls into the polypropylene line of products where a small percentage of ethylene is added to increase clarity. The so-called "block copolymer" is a sequentially polymerized propylene/ethylene product that contains a complex myriad of copolymer structures. Ethylene–propylene rubbers can be produced without inverted propylene sequences und with predominantly isotactic configurations propylene sequences [55]. Such a copolymer is of little interest commercially, but from an analytical viewpoint it is an excellent model system from which to develop a data base as part of an overall study of ethylene–propylene copolymers. One can establish sequence assignments in the ^{13}C-NMR spectrum without ambiguities introduced by inverted propylene sequences und atactic propylene sequences. A ^{13}C-NMR spectrum of such an ethylene–propylene copolymer is reproduced in Fig. 3.

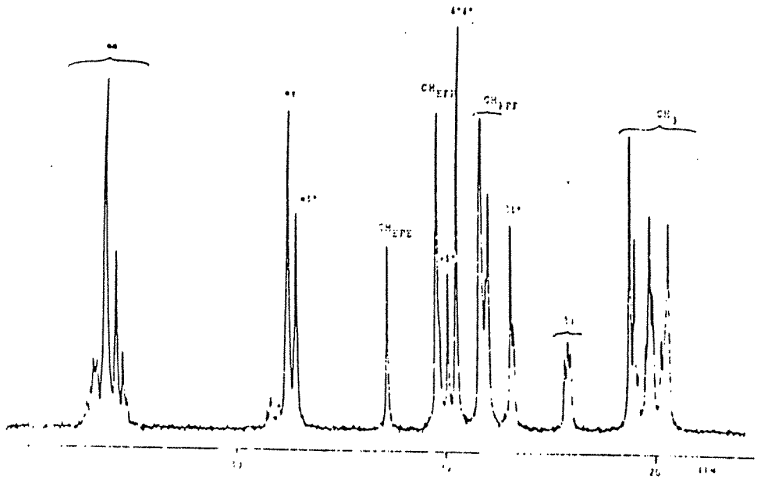

FIG. 3. 50.3 MHz carbon-13 NMR spectrum of an ethylene-propylene copolymer at 125°C in 1,2,4-trichlorobenzene.

and a list of chemical shift assignments is given in Table 6. The nomenclature used in Table 6 is that discussed previously.

Considerable confusion has surrounded the $\alpha\gamma$ and $\alpha\delta^+$ NMR assignments in spectra of ethylene-propylene copolymers [24, 55-59], primarily because of a high sensitivity of these particular methylene carbons to differences in chirality and head-to-tail placements of adjacent propylene repeat units. The most comprehensive summary and definitive assignments are perhaps those of Cheng [59]. Support for Cheng's assignments should be obtained from appropriate model copolymers, of which there are a number that are useful, that is, a predominantly isotactic 99/1 propylene-ethylene copolymer, an atactic 98/2 propylene-ethylene copolymer, a 99/1 ethylene-propylene copolymer, and an alternating ethylene-propylene copolymer, produced by hydrogenation of *cis*-polyisoprene.

The predominantly isotactic 99/1 propylene-ethylene copolymer produces only isolated ethylene repeat units and the following unique sequences involving "E": PPPPE+EPPPP,

TABLE 6

Carbon-13 NMR Chemical Shift Assignments at 50.3 MHz for Ethylene-1-Propylene Copolymers Containing Principally Isotactic Propylene Sequences and No Inverted Propylene Repeat Units. The Samples Were Prepared at 10% by Weight in 1,2,4-Trichlorobenzene (TCB) with Perdeuterobenzene Added and at 15% by Weight in Tetrachloroethane-d_2 (TCE-d_2). The Spectra Were Obtained at 125 ± 1°C. The $\delta^+\delta^+$ Peak Is Set at 29.98 ppm with Respect to an Internal Tetramethylsilane Standard

Chemical shift ppm, TMS			
TCB	TCE-d_2	Carbon assignment	Sequence assignment
46.52	46.60		PPPP (mmm)
46.06	46.16		PPPE+EPPP (mm)
45.77	45.87		EPPE (m)
37.91	37.98		PPPEP+PEPPP (mmm)
37.89	37.94		EPEPE+EPEPE (m)
37.51	37.58	$\alpha\delta^+$	EPEE+EEPE
37.46	37.50	$\alpha\delta^+$	PPEE+EEPP
33.22	33.29	Methine	EPE
30.95	30.97	Methine	EPP+PPE
30.77	30.76	$\gamma\gamma$	PEEP
30.36	30.38	$\gamma\delta^+$	PEEE+EEEP
29.98	29.98	$\delta^+\delta^+$	$(EEE)_n$
28.91	28.97	Methine	PPP
27.43	27.44	$\beta\delta^+$	EPEE+EEPE
27.28	27.30	$\beta\delta^+$	PPEE+EEPP
24.85	24.89	$\beta\beta$	EPEPE (m)
24.71	24.74	$\beta\beta$	EPEPP+PPEPE (mm)
24.56	24.61	$\beta\beta$	PPEPP (mmm)
21.83	21.94	Methyl	PPPPP (mmmm)
21.61	21.72	Methyl	PPPPE+EPPPP (mmm)
20.92	21.02	Methyl	PPPEP+PEPPP (mmm)
19.97	20.11	Methyl	EPE

Case 1:05-cv-00737-JJF Document 160-5 Filed 09/03/2008 Page 37 of 42

EXHIBIT PAGE 001012

PPPEP+PEPPP, PPEPP, PPPE+EPPP, PPEP+PEPP, PPE+EPP, and PEP. The observed chemical shifts and assignments for this 99/1 propylene–ethylene copolymer are given in Table 7. The assignment for αγ, PPEPP (mmm), is clearly established by this model system. The ^{13}C-NMR spectrum of this 99/1 ethylene–propylene copolymer at 50.3 MHz and 125°C is reproduced in Fig. 4.

A second useful model copolymer is a 99/1 ethylene–propylene copolymer. Only sequences involving isolated propylene units will be present with the following sequences uniquely observable: PEEE+EEEP, EPEE+EEPE, PEE+EEP, and EPE. An opportunity is now afforded to assign unequivocally the αδ⁺ EPEE+EEPE sequence as shown in Table 8. The ^{13}C-NMR spectrum of this model copolymer at 50.3 MHz and 125°C is reproduced in Fig. 5. Weak resonances are observed for αγ and ββ sequences, indicating that alternating EPEPE sequences are also present. Even weaker resonances indicate the presence of a small amount of blocked propylene sequences.

A third copolymer system useful for confirming assignments is the alternating ethylene–propylene copolymer produced by hydrogenation of *cis*-polyisoprene.

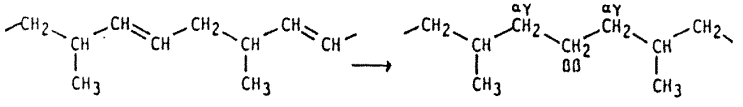

The chemical shifts for the alternating ethylene–propylene copolymer are given in Table 9, and the ^{13}C-NMR spectrum at 50.3 MHz and 125°C is reproduced in Fig. 6. There is a common EPE methine resonance in the spectra of the alternating copolymer and the 99/1 ethylene copolymer that can serve as a chemical shift reference point for these two model systems. To create further standardization of chemical shifts among these various model copolymers, a small amount of polyethylene standard (NBS 1475) was added to create a reference chemical shift at 29.98 ppm. The polyethylene reference was added to the 99/1 propylene–ethylene copolymer and the alternating copolymer so that the data in each of the tables would have a common chemical shift basis.

The sequences observable in the ^{13}C-NMR spectrum of the alternating copolymer are EPEPEPE, EPEPE, and EPE. This

TABLE 7

Carbon-13 NMR Chemical Shift Assignments at 50.3 MHz for a Propylene–Ethylene Copolymer Containing Only One Mole Percent Ethylene and Principally Isotactic Propylene Sequences. The Sample Was Prepared at 10% by Weight in 1,2,4-Trichlorobenzene and the Spectrum Obtained at 125 ± 1°C with Respect to an Internal Tetramethylsilane Standard

Chemical shift ppm, TMS	Carbon assignment	Sequence assignment
46.52	αα	PPPP (mmm)
46.06	αα	PPPE+EPPP (mm)
37.91	αγ	PPEPP (mmm)
30.97	Methine	EPP+PPE (m)
28.93	Methine	PPP (mm)
24.56	βγ	PPEPP (mmm)
21.83	Methyl	PPPPP (mmmm)
21.61	Methyl	PPPPE+EPPPP (mmm)
20.92	Methyl	PPPEP+PEPPP (mmm)

TABLE 8

Carbon-13 NMR Chemical Shift Assignments at 50.3 MHz for an Ethylene–Propylene Copolymer Containing Only One Mole Percent Propylene. The Sample Was Prepared at 10% by Weight in 1,2,4-Trichlorobenzene and the Spectrum Obtained at 125 ± 1°C with Respect to an Internal Tetramethylsilane Standard

Chemical shift ppm, TMS	Carbon assignment	Sequence assignment
37.51	αδ⁺	EPEE+EEPE
33.22	Methine	EPE
30.36	γδ⁺	PEEE+EEEP
29.98	δ⁺δ⁺	$(EEE)_n$
27.42	βδ⁺	EPEE+EEPE
19.96	Methyl	EPE

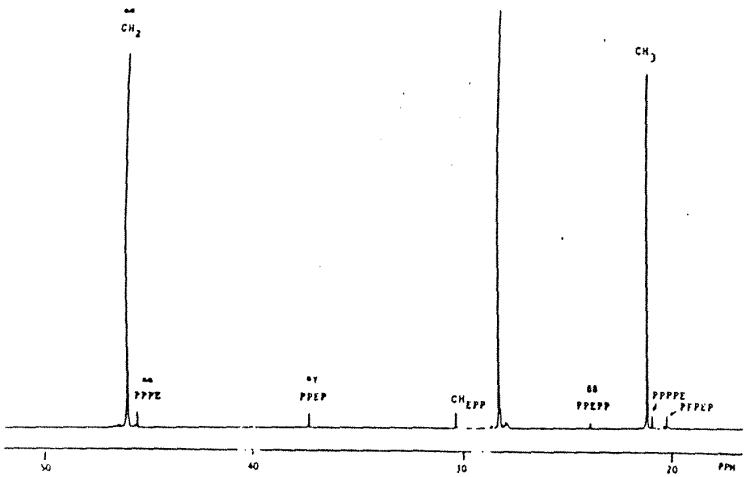

FIG. 4. 50.3 MHz carbon-13 NMR spectrum of an 1/99 ethylene–propylene copolymer at 125°C in 1,2,4-trichlorobenzene.

TABLE 9

Carbon-13 NMR Chemical Shift Assignments at 50.3 MHz for an Alternating Ethylene–Propylene Copolymer Prepared by Hydrogenation of *cis*-Polyisoprene. The Sample Was Prepared at 10% by Weight in 1,2,4-Trichlorobenzene and the Spectrum Obtained at 125 ± 1°C with Respect to an Internal Tetramethylsilane Standard

Chemical shift ppm, TMS	Carbon assignment	Sequence assignment
37.95 r	αγ	EPEPEPE
37.89 m	αγ	EPEPEPE
33.24	Methine	EPE
24.86	ββ	EPEPE
20.02 mm	Methyl	EPEPEPE
19.98 mr+rm	Methyl	EPEPEPE
19.95 rr	Methyl	EPEPEPE

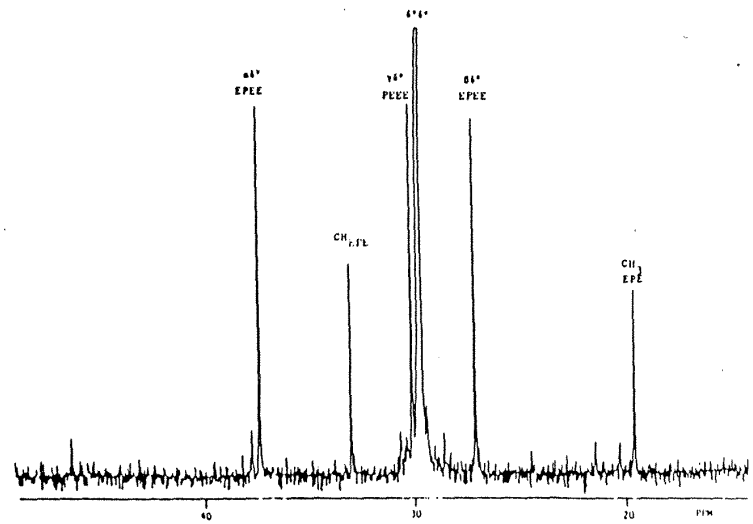

FIG. 5. 50.3 MHz carbon-13 NMR spectrum of a 99/1 ethylene–propylene copolymer at 125°C in 1,2,4-trichlorobenzene.

reference copolymer also permitted the chemical shift differences for meso and racemic PEP methyl groups and EPEPEPE αγ carbons to be established. The 0.06 ppm αγ racemic versus meso chemical shift difference is in agreement with the observations reported by Zetta et al. [60]. The effect of chirality on methyl group resonances from propylene repeat units located on either side of a bridging ethylene unit is quite small as predicted by Tonelli [37]. This is an important consideration when assigning chiral differences for PPEPP sequences. Considering the three carbon γ effect in *gauche* arrangements utilizing a rotational isomeric state model, Tonelli predicted that the downfield αγ carbon resonance would belong to the racemic isomer [37]. The methyl resonances in Fig. 6 show a 1:2:1 splitting pattern with a separation of 0.03–0.04 ppm. Tonelli assigned these methyl chemical shifts to mm, mr+rm, and rr from low to high fields, respectively [37]. No other splittings related to chiral differences were observed among the remaining resonances.

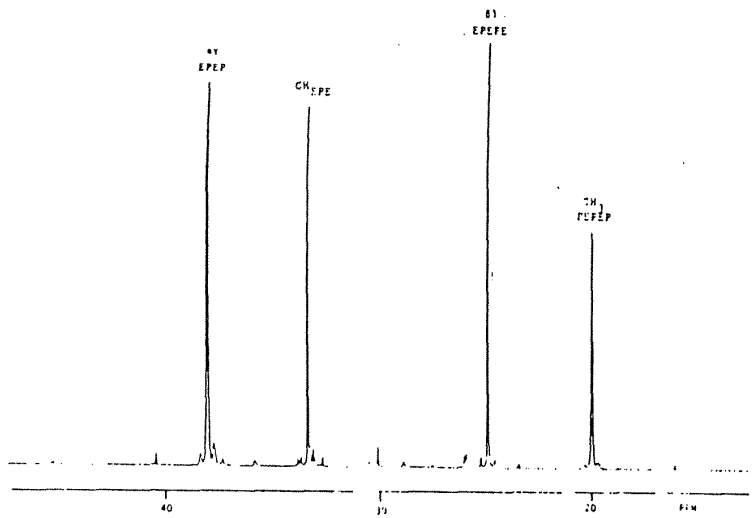

FIG. 6. 50.3 MHz carbon-13 NMR spectrum of a hydrogenated poly-*cis*-1,4-isoprene. The sample, which is an alternating ethylene–propylene copolymer, was run at 125°C in 1,2,4-trichlorobenzene.

It was possible to obtain a fourth model copolymer by removing the room temperature xylene-soluble atactic polypropylene from the principally isotactic 99/1 propylene–ethylene copolymer. The extracted copolymer contained isolated ethylene units as a major constituent, but a few ethylene dimers, trimers, possibly tetramers and alternating sequences are present as indicated by the data in Table 10 and the 50.3 MHz ^{13}C-NMR spectrum in Fig. 7. At least three new αγ types of resonances are clearly visible. Tonelli [38] has established that the PPEPP chiral effects on the center propylene units result from the closest propylene repeat unit and not from the neighboring propylene unit across the ethylene bridge as shown below:

TABLE 10

Carbon-13 NMR Chemical Shift Assignments at 50.3 MHz for an Ethylene–Propylene Copolymer Containing Approximately One Mole Percent Ethylene and Principally Atactic Propylene Sequences. Peak Heights Are Given in Millimeters. The Sample Was Prepared at 10% by Weight in 1,2,4-Trichlorobenzene and the Spectrum Obtained at 125 ± 1°C with Respect to an Internal Tetramethylsilane Standard

Chemical shift ppm, TMS	Peak height	Carbon assignment	Sequence assignment
38.95	9	αγ	PPPEP+PEPPP r_1r_2
38.75	17	αγ	PPPEP+PEPPP r_1m_2
38.09	18	αγ	PPEP+PEPP m_1r_2
37.98	41	αγ	PEPEP (r)
37.94	67	αγ	PPPEP+PEPPP m_1m_2
37.56	11	$\alpha\delta^+$	EPEE+EEPE
37.50	9	$\alpha\delta^+$	PPEE+EEPP
33.27	18	Methine	EPE
30.98	71	Methine	EPP+PPE
30.93	56	Methine	EPP+PPE
30.88	49	Methine	EPP+PPE
30.41	6		PEEE+EEEP
29.98	16	$\delta^+\delta^+$	$(EEE)_n$
24.87	7	ββ	"EPEPE" (no m,r assignments)
24.81	10	ββ	
24.72	17	ββ	"EPEPP+PPEPE"
24.68	15	ββ	
24.64	14	ββ	
24.59	26	ββ	"PPEPP"

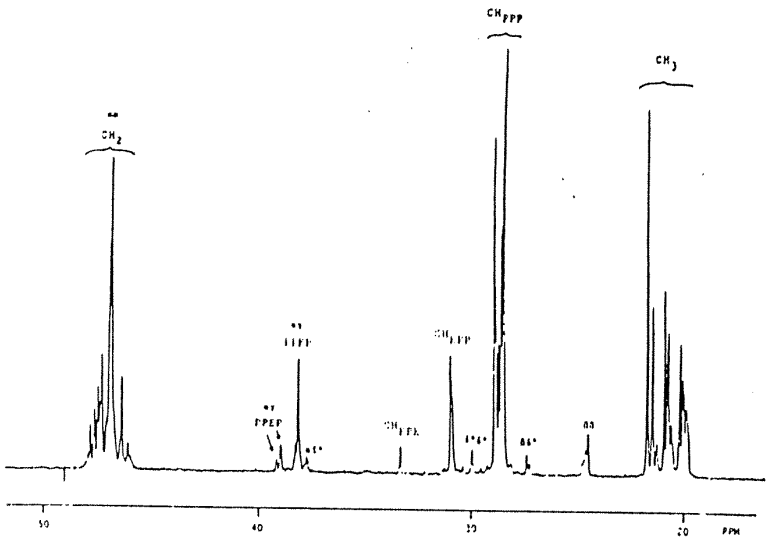

FIG. 7. 50.3 MHz carbon-13 NMR spectrum of a 99/1 ethylene–propylene copolymer containing principally atactic propylene sequences at 125°C in 1,2,4-trichlorobenzene.

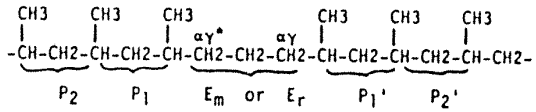

A * is used to designate the $\alpha\gamma$ carbon that defines the relationships, P_1, P_2, P_1', and P_2'. This $\alpha\gamma$* chemical shift is influenced by P_1 and P_2 but not significantly by P_1'. Consequently, P_2' has no effect. A calculation of the effect of the chirality of P_1 on the $\alpha\gamma$* carbon chemical shift by Tonelli, utilizing the rotational isomeric state model and γ effects from

gauche conformations, has shown that a racemic P_1 diad deshields the $\alpha\gamma$ carbon resonance by approximately 1–1.5 ppm [38]. The observed m versus r chemical shift difference for P_1 is 0.8 to 0.9 ppm in Table 10. The assignments for the effect of P_2 follow because it is expected to be considerably less than P_1 with r_2 being downfield from m_2. The four stereochemical assignments for PPEP+PEPP sequences are given in Table 10. The m versus r P_2 effect is 0.1 to 0.2 ppm.

The only $\alpha\gamma$ resonance not observed in the spectrum shown in Fig. 7 is EPEP+PEPE (m), which probably overlaps with PPEP+PEPP m_1m_2 as indicated by the chemical shift data in Table 9. It is also clear from the data in Table 9 versus Table 10 that the EPP+PPE methine chemical shift is sensitive to P_1 and P_2 but not either to E_m, E_r, P_1', or P_2'.

The assignments given in Table 6 and Table 10 appear to be well supported by the model copolymers and the calculations of Tonelli. The $\alpha\delta^+$ PPEE+EEPP assignment is made by default and should remain tentative. As far as the remaining ^{13}C-NMR resonance assignments in ethylene–propylene copolymer spectra are concerned, there has been general agreement among various workers in the field.

It is clear from this discussion of assignments that the basic types of methylenes can easily be assigned by several techniques. Difficulties lie in assignments of subtle chemical shift differences created by differences in chirality or a specific sensitivity to a higher order *n*-ad sequence length within sequences of the same basic type. In quantitative treatments it is possible to include these subtleties without making specific assignments by reducing the information to a distribution over a shorter *n*-ad sequence length. As discussed earlier, a complete sequence distribution independently over either diads, triads or tetrads, etc. will lead to comonomer mole fractions, average sequence lengths for each monomer type, run numbers, and sequence numbers. An inspection of the data in Table 6 shows that an NMR spectrum of a predominantly isotactic ethylene–propylene copolymer gives potential quantitative information directly for six different pentads, ten different tetrads, and three different triads. A complete pentad, tetrad, or triad distribution cannot be determined directly from the NMR spectrum. Complete triad and tetrad distributions can be obtained if one combines the observed information with an imaginative use of the necessary relationships

Case 1:05-cv-00737-JJF Document 160-5 Filed 09/03/2008 Page 41 of 42
EXHIBIT PAGE 001016

given in Table 1. The necessary relationships will allow specific resonances to be combined, thus allowing more accurate spectral integrations over well-resolved regions. Ambiguities associated with resonance overlap and uncertainties in assignments can therefore be avoided. This procedure can best be understood through the following quantitative determination of the complete triad sequence distribution in ethylene–propylene copolymers.

The initial step in a quantitative treatment is to divide the spectrum into spectral regions, A through "X," as dictated by overlap and necessary relationship considerations. Such regions are described below according to range in ppm and contributing n-ad sequences. The total resonance area for each region is designated as T_X, where "X" is A, B, C, etc. The final step is to reduce the various n-ad sequence data for each region to a combination of appropriate triads.

Region "A" Range: 45–48 ppm
Contributing carbons: S_α Methylene
Observed n-ads: PPPP, PPPE+EPPP, EPPE

$$T_A = k(PPPP + PPPE+EPPP + EPPE) \quad (28)$$

$$= k(PP) \quad (29)$$

$$= k(PPP + (1/2)[PPE+EPP]) \quad (30)$$

Equations (29) and (30) follow from the necessary relationships between tetrads, diads and diads, triads, respectively. The factor k is the NMR proportionality constant relating the observed resonance intensities to the number of contributing molecular species. It can be later removed through normalization once a complete set of n-ads is obtained or by obtaining the k value for one carbon atom per polymer molecule, which leads directly to the number of contributing n-ads per average polymer chain. Endgroup resonances from linear chains, as in the case for high-density polyethylene, are useful for establishing the value of k for a single carbon atom per chain. Elimination of k by normalization leads to the triad distribution per average polymer chain. A distinct advantage of NMR quantitative analyses over other spectroscopic methods is that the resonance intensities are directly proportional to the number of contributing species, and this proportionality constant remains the same throughout any given spectrum.

Region "B" Range: 36–39 ppm
Contributing carbons: S_γ, $S\delta^+$
Observed n-ads: EPEP+PEPE, PPEP+PEPP EPEE+EEPE, PPEE+EEPP

$$T_B = k(EPEP+PEPE + PPEP+PEPP + EPEE+EEPE + PPEE+EEPP) \quad (31)$$

$$= k(PE+EP) \quad (32)$$

$$= k(2PEP + PEE+EEP) = k(2EPE + EPP+PPE) \quad (33)$$

$$= k(PEP + (1/2)[PEE+EEP] + EPE + (1/2)[EPP+PPE]) \quad (34)$$

Once again, the region is defined in terms of contributing diads, triads, and tetrads by invoking the appropriate necessary relationships. Note that any ambiguities in the S_γ and $S\delta^+$ assignments have been avoided through a collective treatment of the entire region. Also, any errors introduced through configurational "splittings" have been avoided if contained within the region, as appears reasonable in these cases.

Region "C" Range: 33.3 ppm
Contributing carbons: $(\text{Methine})_{EPE}$
Observed n-ads: EPE

$$T_C = k(EPE) \quad (35)$$

Region "D" Range: 29.1–31.5 ppm
Contributing carbons: $(\text{Methine})_{EPP+PPE}$, $S\gamma S\gamma$, $S\gamma S\delta^+$, $S\delta^+S\delta^+$
Observed n-ads: EPP+PPE, PEEP, PEEE+EEEP, $(EEE)_n$

The following special relationship is also required to define the "D" area in terms of triads:

$$EEE = (1/2)S^+\delta^+ + (1/4)S\delta^+ \quad (36)$$